

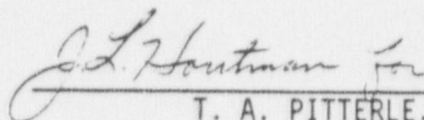
WCAP-12142

BEAVER VALLEY UNIT 2
EVALUATION FOR TUBE VIBRATION INDUCED FATIGUE

FEBRUARY 1989

| | | |
|----------|---------------|--------------|
| AUTHORS: | H. J. CONNORS | A. Y. LEE |
| | J. M. HALL | T. S. MAGGE |
| | G. W. HOPKINS | A. C. SMITH |
| | J. L. HOUTMAN | R. M. WILSON |
| | M. H. HU | H. W. YANT |

APPROVED:



T. A. PITTERLE, MANAGER
STEAM GENERATOR ENGINEERING

WORK PERFORMED UNDER SHOP ORDER PG8D52274

This document contains information proprietary to Westinghouse Electric Corporation. It is submitted in confidence and is to be used solely for the purpose for which it is furnished and is to be returned upon request. This document and such information is not to be reproduced, transmitted, disclosed or used otherwise in whole or in part without written authorization of Westinghouse Electric Corporation, Power Systems Business Unit.

WESTINGHOUSE ELECTRIC CORPORATION
SERVICE TECHNOLOGY DIVISION
P.O. BOX 3377
PITTSBURGH, PENNSYLVANIA 15230

0307M:49/022789-1

8904120396 890406
PDR ADOCK 05000412
Q PDC

ABSTRACT

On July 15, 1987, a steam generator tube rupture event occurred at the North Anna Unit 1 plant. The cause of the tube rupture has been determined to be high cycle fatigue. The source of the loads associated with the fatigue mechanism is a combination of a mean stress level in the tube with a superimposed alternating stress. The mean stress is the result of manufacturing residual stress, applied stress and residual stress due to denting of the tube at the top tube support plate, while the alternating stress is due to out-of-plane deflection of the tube U-bend attributed to flow induced vibration. For tubes without AVB support, local flow peaking effects at unsupported tubes are a significant contribution to tube vibration amplitudes.

This report documents the evaluation of steam generator tubing at Beaver Valley Unit 2 for susceptibility to fatigue-induced cracking of the type experienced at North Anna Unit 1. The evaluation utilizes operating conditions specific to Beaver Valley Unit 2 to account for the plant specific nature of the tube loading and response. The evaluation also includes reviews of eddy current data for Beaver Valley Unit 2 to establish AVB locations. This report provides background of the event which occurred at North Anna, a criteria for fatigue assessment, a summary of test data which support the analytical approach, field measurement results showing AVB positions, thermal hydraulic analysis results, and calculations to determine tube mean stress, stability ratio and tube stress distributions, and accumulated fatigue usage. This evaluation concludes that one of the tubes in Steam Generator B, and two tubes in Steam Generator C are potentially susceptible to fatigue and require corrective action.

SUMMARY OF ABBREVIATIONS

| | |
|--------|--|
| ASME | - American Society of Mechanical Engineers |
| ATHOS | - Analysis of the Thermal Hydraulics of Steam Generators |
| AVB | - Anti-Vibration Bar |
| AVT | - All Volatile Treatment |
| ECT | - Eddy Current Test |
| EPRI | - Electric Power Research Institute |
| FFT | - Fast Fourier Transform |
| FLOVIB | - Flow Induced Vibrations |
| MEVF | - Modal Effective Void Fraction |
| OD | - Outside Diameter |
| RMS | - Root Mean Square |
| SR | - Stability Ratio |
| TSP | - Tube Support Plate |
| | |
| *F | - degrees Fahrenheit |
| hr | - hour |
| ksi | - measure of stress - 1000 pounds per square inch |
| lb | - pound |
| mils | - 0.001 inch |
| MW | - megawatt |
| psi | - measure of stress - pounds per square inch |
| psia | - measure of pressure - absolute |

TABLE OF CONTENTS

SECTION

- 1.0 Introduction

- 2.0 Summary and Conclusions
 - 2.1 Background
 - 2.2 Evaluation Criteria
 - 2.3 Denting Evaluation
 - 2.4 AVB Insertion Depths
 - 2.5 Flow Peaking Factors
 - 2.6 Tube Vibration Evaluation
 - 2.7 Overall Conclusion

- 3.0 Background
 - 3.1 North Anna Unit 1 Tube Rupture Event
 - 3.2 Tube Examination Results
 - 3.3 Mechanism Assessment

- 4.0 Criteria for Fatigue Assessment
 - 4.1 Stability Ratio Reduction Criteria
 - 4.2 Local Flow Peaking Considerations
 - 4.3 Stress Ratio Considerations

- 5.0 Supporting Test Data
 - 5.1 Stability Ratio Parameters
 - 5.2 Tube Damping Data
 - 5.3 Tube Vibration Amplitudes with Single-Sided AVB Support
 - 5.4 Tests to Determine the Effects on Fluidelastic Instability of Columnwise Variations in AVB Insertion Depths
 - 5.5 References

TABLE OF CONTENTS (CONTINUED)

SECTION

- 6.0 Eddy Current Data and AVB Positions
 - 6.1 AVB Assembly Design
 - 6.2 Eddy Current Data for AVB Positions
 - 6.3 Tube Denting at Top Tube Support Plate
 - 6.4 AVB Map Interpretations

- 7.0 Thermal and Hydraulic Analysis
 - 7.1 Beaver Valley Unit 2 Steam Generator Operating Conditions
 - 7.2 ATHOS Analysis Model
 - 7.3 ATHOS Results
 - 7.4 Relative Stability Ratio Over Operating History

- 8.0 Peaking Factor Evaluation
 - 8.1 North Anna 1 Configuration
 - 8.2 Test Measurement Uncertainties
 - 8.3 Test Repeatability
 - 8.4 Cantilever vs U-Tube
 - 8.5 Air vs Steam Water Mixture
 - 8.6 AVB Insertion Depth Uncertainty
 - 8.7 Overall Peaking Factor with Uncertainty

- 9.0 Structural and Tube Vibration Assessments
 - 9.1 Tube Mean Stress
 - 9.2 Stability Ratio Distribution Based Upon ATHOS
 - 9.3 Stress Ratio Distribution with Peaking Factor
 - 9.4 Cumulative Fatigue Usage

LIST OF FIGURES

FIGURE

- 3-1 Approximate Mapping of Fracture Surface of Tube R9C51 S/G "C"
Cold Leg, North Anna Unit 1
- 3-2 Schematic Representation of Features Observed During TEM
Fractographic Examination of Fracture Surface of Tube R9C51, S/G
"C" Cold Leg, North Anna Unit 1
- 3-3 Calculated and Observed Leak Rates Versus Time
- 4-1 Vibration Displacement vs. Stability Ratio
- 4-2 Fatigue Strength of Inconel 600 in AVT Water at 600°F
- 4-3 Fatigue Curve for Inconel 600 in AVT Water Comparison of Mean Stress
Correction Models
- 4-4 Modified Fatigue with 10% Reduction in Stability Ratio for
Maximum Stress Condition
- 4-5 Modified Fatigue with 5% Reduction in Stability Ratio for
Minimum Stress Condition
- 5-1 Fluidelastic Instability Uncertainty Assessment
- 5-2 Instability Constant - β
- 5-3 Instability Constants, β , Obtained for Curved Tube from Wind Tunnel
Tests on the 0.214 Scale U-Bend Model
- 5-4 Damping vs. Slip Void Fraction

LIST OF FIGURES (Continued)

FIGURE

- 5-5 Overall View of Cantilever Tube Wind Tunnel Model
- 5-6 Top View of the Cantilever Tube Wind Tunnel Model
- 5-7 Fluidelastic Vibration Amplitude with Non-Uniform Gaps
- 5-8 Typical Vibration Amplitude and Tube/AVB Impact Force Signals for Fluidelastic Vibration with Unequal Tube/AVB Gaps
- 5-9 Conceptual Design of the Apparatus for Determining the Effects on Fluidelastic Instability of Columnwise Variations in AVB Insertion Depths
- 5-10 Overall View of Wind Tunnel Test Apparatus
- 5-11 Side View of Wind Tunnel Apparatus with Cover Plates Removed to Show Simulated AVBS and Top Flow Screen
- 5-12 AVB Configurations Tested
- 5-13 Typical Variation of RMS Vibration Amplitude with Flow Velocity for Configuration 1a in Figure 5-12
- 6-1 AVB Insertion Depth Confirmation
- 6-2 Beaver Valley Unit 2 - Steam Generator A - AVB Positions
- 6-3 Beaver Valley Unit 2 - Steam Generator B - AVB Positions
- 6-4 Beaver Valley Unit 2 - Steam Generator C - AVB Positions

LIST OF FIGURES (Continued)

FIGURE

- 7-1 Plan View of ATHOS Cartesian Model for Beaver Valley Unit 2
- 7-2 Elevation View of ATHOS Cartesian Model for Beaver Valley Unit 2
- 7-3 Plan View of ATHOS Cartesian Model Indicating Tube Layout
- 7-4 Flow Pattern on Vertical Plane of Symmetry
- 7-5 Vertical Velocity Contours on a Horizontal Plane at the Entrance to the U-Bend
- 7-6 Lateral Flow Pattern on Horizontal Plane at the Entrance to the U-Bend
- 7-7 Void Fraction Contours on Vertical Plane of Symmetry
- 7-8 Tube Gap Velocity and Density Distributions for Tube at R10/C3
- 7-9 Tube Gap Velocity and Density Distributions for Tube at R10/C20
- 7-10 Tube Gap Velocity and Density Distributions for Tube at R10/C40
- 7-11 Average Velocity and Density in the Plane of the U-Bends Normal to Row 10
- 7-12 Beaver Valley Unit 2 Normalized Stability Ratio Based on High Power (>85%) Operation

LIST OF FIGURES (Continued)

FIGURE

- 8-1 Original North Anna AVB Configuration
- 8-2 Schematic of Staggered AVBs
- 8-3 AVB "Pair" in ECT Trace
- 8-4 North Anna 1, Steam Generator C: AVB Positions Critical Review "AVB Visible" Calls
- 8-5 North Anna 1, Steam Generator C, R9C51 Projection Matrix
- 8-6 North Anna R9C51 AVB Final Projected Positions
- 8-7 Final Peaking Factors for Beaver Valley Unit 2
- 9-1 Axisymmetric Tube Finite Element Model
- 9-2 Dented Tube Stress Distributions - Pressure Load on Tube
- 9-3 Dented Tube Stress Distributions - Interference Load on Tube
- 9-4 Dented Tube Stress Distributions - Combined Stress Results
- 9-5 Relative Stability Ratio vs. Column Number for MEVF Dependent Damping - Beaver Valley Unit 2
- 9-6 Stress Ratio Vs. Column Number for Dented Condition - Beaver Valley Unit 2
- 9-7 Stress Ratio Vs. Column Number for Undented Condition - Beaver Valley Unit 2
- 9-8 Beaver Valley Unit 2 - Maximum Allowable Relative Flow Peaking

LIST OF TABLES

TABLE

- 4-1 Fatigue Usage per Year Resulting From Stability Ratio Reduction
- 5-1 Wind Tunnel Test on Cantilever Tube Model
- 5-2 Fluidelastic Instability Peaking Velocity Factors for Columnwise Variations in AVB Insertion Depths
- 6-1 Summary Listing of Unsupported Tubes - Beaver Valley Unit 2
- 7-1 Beaver Valley Unit 2 Steam Generator Operating Conditions Used for ATHOS Analysis
- 7-2 Beaver Valley Unit 2 Operating History Data
- 8-1 Stability Peaking Factor Due to Local Velocity Perturbation
- 8-2 Comparison of Air and Steam-Water Peaking Factor Ratios
- 8-3 Effect of Local Variation of AVB Insertion
- 8-4 Uncertainties in Test Data and Extrapolation
- 8-5 Extrapolation of Test Results to Steam Generator Conditions
- 8-6 Final Peaking Factors
- 8-7 Stability Peaking Factors for Specific Tubes
- 9-1 100% Power Operating Parameters
- 9-2 Summary of Beaver Valley Unit 2 Evaluation of the Salient Unsupported U-Bends

1.0 INTRODUCTION

This report documents the evaluation of steam generator tubing at Beaver Valley Unit 2 for susceptibility to fatigue-induced cracking of the type experienced at North Anna Unit 1 in July, 1987. The evaluation includes three-dimensional flow analysis of the tube bundle, air-tests performed to support the vibration analytical procedure, field measurements to establish AVB locations, structural and vibration analysis of selected tubes, and fatigue usage calculations to predict cumulative usage for critical tubes. The evaluation utilizes operating conditions specific to Beaver Valley Unit 2 in order to account for plant specific features of the tube loading and response.

Section 2 of the report provides a summary of the Beaver Valley Unit 2 evaluation results and overall conclusions. Section 3 provides background for the tube rupture event which occurred at North Anna Unit 1 including results of the examination of the ruptured tube and a discussion of the rupture mechanism. The criteria for predicting the fatigue usage for tubes having an environment conducive to this type of rupture are discussed in Section 4. Section 5 provides a summary of test data which supports the analytical vibration evaluation of the candidate tubes. A summary of field measurements used to determine AVB locations and to identify unsupported tubes is provided in Section 6. Section 7 provides the results of a thermal hydraulic analysis to establish flow field characteristics at the top support plate which are subsequently used to assist in identifying tubes which may be dynamically unstable. Section 8 presents an update of the methodology originally used to evaluate the tube rupture at North Anna Unit 1. The final section, Section 9, presents results of the structural and vibration assessment. This section describes tube mean stress, stability ratio and tube stress distributions, and accumulated fatigue usage, for the small radius U-tubes in the Beaver Valley Unit 2 steam generators.

2.0 SUMMARY AND CONCLUSIONS

The Beaver Valley Unit 2 steam generators have been evaluated for the susceptibility of unsupported U-bend tubing with denting at the top tube support plate to a fatigue rupture of the type experienced at Row 9 Column 51 (R9C51) of Steam Generator C at North Anna Unit 1. The evaluation used Eddy Current Test (ECT) data supplied by Duquesne Light Company, and interpreted by Westinghouse.

2.1 Background

The initiation of the circumferential crack in the tube at the top of the top tube support plate at North Anna 1 has been attributed to limited displacement, fluid elastic instability. This condition is believed to have prevailed in the R9C51 tube since the tube experienced denting at the support plate. A combination of conditions were present that led to the rupture. The tube was not supported by an anti-vibration bar (AVB), had a higher flow field due to local flow peaking as a result of non-uniform insertion depths of AVBs, had reduced damping due to denting at the top support plate, and had reduced fatigue properties due to the environment of the all volatile treatment (AVT) chemistry of the secondary water and the additional mean stress from the denting.

2.2 Evaluation Criteria

The criteria established to provide a fatigue usage less than 1.0 for a finite period of time (i.e., 40 years) is a 10% reduction in stability ratio that provides at least a 58% reduction in stress amplitude (to < 4.0 ksi) for a Row 9 tube in the North Anna 1 steam generators (SG's). A reduction of this magnitude is required to produce a fatigue usage of < 0.021 per year for a Row 9 tube in North Anna and therefore a fatigue life objective of greater than 40 years. This same fatigue criteria is applied as the principal criteria in the evaluation of Beaver Valley Unit 2 tubing.

The fluidelastic stability ratio is the ratio of the effective velocity divided by the critical velocity. A value greater than unity (1.0) indicates instability. The stress ratio is the expected stress amplitude in a Beaver Valley Unit 2 tube divided by the stress amplitude for the North Anna 1, R9C51 tube.

Displacements are computed for the unsupported U-bend tubes in Rows 11 and inward, (descending row number) using relative stability ratios to R9C51 of North Anna 1 and an appropriate power law relationship based on instability displacement versus flow velocity. Tubes having different U-bend radii will have different stiffness and frequency and, therefore, different stress and fatigue usage per year than the Row 9 North Anna tube. These effects are accounted for in a stress ratio technique. The stress ratio is formulated so that a stress ratio of 1.0 or less produces acceptable stress amplitudes and fatigue usage for the Beaver Valley Unit 2 tubing for the reference fuel cycle analyzed. Therefore, a stress ratio less than 1.0 provides the next level of acceptance criteria for unsupported tubes for which the relative stability ratio, including flow peaking, exceed 0.9.

The stability ratios for Beaver Valley Unit 2 tubing, the corresponding stress and amplitude, and the resulting cumulative fatigue usage must be evaluated relative to the ruptured tube at Row 9 Column 51, North Anna 1, Steam Generator C, for two reasons. The local effect on the flow field due to various AVB insertion depths is not within the capability of available analysis techniques and is determined by test as a ratio between two AVB configurations. In addition, an analysis and examination of the ruptured tube at North Anna 1 provided a range of initiating stress amplitudes, but could only bound the possible stability ratios that correspond to these stress amplitudes. Therefore, to minimize the influence of uncertainties, the evaluation of Beaver Valley Unit 2 tubing has been based on relative stability ratios, relative flow peaking factors, and relative stress ratios.

The criteria for establishing that a tube has support from an AVB and therefore eliminate it from further considerations is that it must have at least one sided AVB support present at the tube centerline. The criteria is based on test results which show that one sided AVB support is sufficient to limit the

vibration amplitude for fluidelastic excitation. AVB support is established by analysis of eddy current (EC) measurements and is a key factor in the determining the local flow peaking factors. The local flow peaking produces increased local velocities which cause an increase in stability ratio. A small percentage change in the stability ratio causes a significant change in stress amplitude. The relative flow peaking factors for Beaver Valley Unit 2 tubing without direct AVB support have been determined by test. These flow peaking factors normalized to the North Anna R9C51 peaking, are applied to relative stability ratios determined by 3-D tube bundle flow analysis, to obtain the combined relative stability ratio used in the stress ratio determination.

2.3 Denting Evaluation

The Eddy Current (EC) tapes used by Westinghouse in the evaluation were those generated in August and September of 1985 as part of the "Baseline" documentation. Naturally this EC data shows no indication of corrosion or magnetite at the tube/TSP interfaces. However, for conservatism in the evaluation, all of the tubes are evaluated for two possible conditions - corroded, but not dented; and as being dented. The effect of denting on the fatigue usage of the tube has been conservatively maximized by assuming the maximum effect of mean stress in the tube fatigue usage evaluation and by incorporating reduced damping in the tube vibration evaluation.

2.4 AVB Insertion Depths

The Beaver Valley Unit 2 SGs have two sets of Alloy 600 AVBs. The 'inner' AVBs have a rectangular cross-section and extend into the tube bundle approximately as far as Row 11. Discounting tube ovality, which tends to vary with bend radius, they provide a nominal total clearance between a given tube and the surrounding AVBs of []^{a,C} inch. Considering average tube ovality for a Row 11 tube, the nominal total tube to AVB clearance is approximately []^{a,C} inches.

The outer AVBs, have the same cross section as the inner AVBs, and extend into the tube bundle approximately as far as Row 14, providing a nominal tube to AVB clearance comparable to the inner AVBs. Since the purpose of this analysis is

to evaluate the potentially unsupported tubes at or near the point of maximum AVB insertion, only the dimensions and EC data pertaining to the inner AVBs are required.

The eddy current data supplied by Duquesne Light were reviewed by Westinghouse to identify the number of tube/AVB intersections and the location of these intersections relative to the apex of a given tube. This information was used in calculations by Westinghouse to determine the deepest penetration of a given AVB into the tube bundle. For the area of interest in the Beaver Valley Unit 2 steam generators, the AVB support of the tube can normally be verified if EC data shows both legs of the lower AVB, one on each side (hot leg - cold leg) of the U-bend. This data, indicated by a listing of two or more AVBs in the insertion depth plots, is the method of choice for establishing tube support.

If only the apex of an AVB assembly is near or touching the apex of a tube U-bend, only one AVB signal may be seen. In this case, adequate tube support cannot be assumed without supplemental input. Support can be determined if 'projection' calculations based on the AVB intercepts of higher row number tubes for the same column verify insertion depth to a point below the tube centerline. Maps of the AVB insertion depths for Beaver Valley Unit 2 are shown in Figures 6-2 thru 6-5. These AVB maps list the results of the 'projection' calculations where this information contributes to understanding of the AVB insertion depth.

2.5 Flow Peaking Factors

Tests were performed modeling Beaver Valley Unit 2, Series 51 SG tube and AVB geometries to determine the flow peaking factors for various AVB configurations relative to the North Anna R9C51 peaking factor. The test results were used to define an upper bound of the ratio relative to the R9C51 configuration. It was found that one tube in SG-B of Beaver Valley Unit 2, and two tubes in SG-C had flow peaking values of the same order of magnitude as R9C51.

2.6 Tube Vibration Evaluation

The calculation of relative stability ratios for Beaver Valley Unit 2 makes use of detailed tube bundle flow field information computed by the ATHOS steam

generator thermal/hydraulic analysis code. Code output includes three-dimensional distributions of secondary side velocity, density, and void fraction, along with primary fluid and tube wall temperatures. Distributions of these parameters have been generated for every tube of interest in the Beaver Valley Unit 2 tube bundles based on recent full power operating conditions. This information was factored into the tube vibration analysis leading to the relative stability ratios.

Relative stability ratios of Beaver Valley Unit 2 (Row 8 through Row 12) tubing versus R9C51 of North Anna 1 are plotted in Figure 9-5 and 9-6, respectively. These relative stability ratios include relative flow peaking factors. The stress ratios for Beaver Valley Unit 2 are given in Figure 9-7. These also include the relative flow peaking effect, and are calculated based on clamped tube conditions with denting at the tube support plate.

Examination of Table 9.2 and Figure 9-6 shows that the unsupported tubes at R11C4 and R9C33 of SG-C exceed the limiting stress ratio criteria, and should be plugged. It is recommended that these tubes be plugged using sentinel plugs.

Of the remaining unsupported tubes in all three SGs, the highest stress ratio is 0.78 and occurs at location R9C60 in SG A. Combining the usage for the operating history to date plus the projected usage for the future operation, assuming operation at 100% power with the current parameters and plugging values for 100% availability, the maximum calculated fatigue usage is 0.40. Since the fatigue usage for this tube is less than 1.0, all analyzed tubing (with the exception identified above) in Beaver Valley Unit 2 is acceptable for continued service.

2.7 Overall Conclusion

The analysis described above indicates that the Beaver Valley Unit 2 tubes recommended to remain in service are not expected to be susceptible to fatigue rupture at the top support plate in a manner similar to the rupture which occurred at North Anna 1. Therefore, no modification, preventive tube plugging, or other measure to preclude such an event is necessary in other than the plugging of R11C4 and R9C33 of SG C.

3.0 BACKGROUND

On July 15, 1987, a steam generator tube rupture occurred at the North Anna Unit 1. The ruptured tube was determined to be Row 9 Column 51 in steam generator "C". The location of the opening was found to be at the top tube support plate on the cold leg side of the tube and was circumferential in orientation with a 360 degree extent.

3.1 North Anna Unit 1 Tube Rupture Event

The cause of the tube rupture has been determined to be high cycle fatigue. The source of the loads associated with the fatigue mechanism has been determined to be a combination of a mean stress level in the tube and a superimposed alternating stress. The mean stress has been determined to have been increased to a maximum level as the result of denting of the tube at the top tube support plate and the alternating stress has been determined to be due to out-of-plane deflection of the tube U-bend above the top tube support caused by flow induced vibration. These loads are consistent with a lower bound fatigue curve for the tube material in an AVT water chemistry environment. The vibration mechanism has been determined to be fluid elastic, based on the magnitude of the alternating stress.

A significant contributor to the occurrence of excessive vibration is the reduction in damping at the tube-to-tube support plate interface caused by the denting. Also, the absence of antivibration bar (AVB) support has been concluded to be required for requisite vibration to occur. The presence of an AVB support restricts tube motion and thus precludes the deflection amplitude required for fatigue. Inspection data shows that an AVB is not present for the Row 9 Column 51 tube but that the actual AVB installation depth exceeded the minimum requirements in all cases with data for AVBs at many other Row 9 tubes. Also contributing significantly to the level of vibration, and thus loading, is the local flow field associated with the detailed geometry of the steam generator, i.e., AVB insertion depths. In addition, the fatigue properties of the tube reflect the lower range of properties expected for an

AVT environment. In summary, the prerequisite conditions derived from the evaluations were concluded to be:

Fatigue Requirements

Prerequisite Conditions

Alternating stress

Tube vibration

- Dented support
- Flow excitation
- Absence of AVB

Mean stress

Denting in addition to applied stress

Material fatigue properties

AVT environment

- Lower range of properties

3.2 Tube Examination Results

Fatigue was found to have initiated on the cold leg outside surface of Tube R9C51 immediately above the top tube support plate. No indications of significant accompanying intergranular corrosion was observed on the fracture face or on the immediately adjacent OD surfaces. Multiple fatigue initiation sites were found with major sites located at 110°, 120°, 135° and 150°, Figure 3-1. The plane of the U-bend is located at 45° with the orientation system used, or approximately 90° from the geometric center of the initiation zone at Section D-D. High cycle fatigue striation spacings approached 1 micro-inch near the origin sites, Figure 3-2. The early crack front is believed to have broken through-wall from approximately 100° to 140°. From this point on, crack growth is believed (as determined by striation spacing, striation direction, and later observations of parabolic dimples followed by equiaxed dimples) to have accelerated and to have changed direction with the resulting crack front running perpendicular to the circumferential direction.

3.3 Mechanism Assessment

To address a fatigue mechanism and to identify the cause of the loading, any loading condition that would cause cyclic stress or steady mean stress had to be considered. The analysis of Normal, Upset and Test conditions indicated a relatively low total number of cycles involved and a corresponding low fatigue usage, even when accounting for the dented tube condition at the plate. This analysis also showed an axial tensile stress contribution at the tube OD a short distance above the plate from operating pressure and temperature, thus providing a contribution to mean stress. Combining these effects with denting deflection on the tube demonstrated a high mean stress at the failure location. Vibration analysis for the tube developed the characteristics of first mode, cantilever response of the dented tube to flow induced vibration for the uncracked tube and for the tube with an increasing crack angle, beginning at 90° to the plane of the tube and progressing around on both sides to complete separation of the tube.

Crack propagation analysis matched cyclic deformation with the stress intensities and striation spacings indicated by the fracture inspection and analysis. Leakage data and crack opening analysis provided the relationship between leak rate and circumferential crack length. Leakage versus time was then predicted from the crack growth analysis and the leakage analysis with initial stress amplitudes of 5, 7, and 9 ksi. The comparison to the best estimate of plant leakage (performed after the event) showed good agreement, figure 3-3.

Based on these results, it followed that the predominant loading mechanism responsible is a flow-induced, tube vibration loading mechanism. It was shown that of the two possible flow-induced vibration mechanisms, turbulence and fluidelastic instability, that fluidelastic instability was the most probable cause. Due to the range of expected initiation stress amplitudes (4 to 10 ksi), the fluidelastic instability would be limited in displacement to a range of approximately []^{a,c}. This is less than the distance between tubes at the apex, []^{a,c}. It was further confirmed that displacement prior to the rupture was limited since no indication of tube U-bend (apex region) damage was evident in the eddy-current signals for adjacent tubes.

Given the likelihood of limited displacement, fluidelastic instability, a means of establishing the change in displacement, and corresponding change in stress amplitude, was developed for a given reduction in stability ratio (SR). Since the rupture was a fatigue mechanism, the change in stress amplitude resulting from a reduction in stability ratio was converted to a fatigue usage benefit through the use of the fatigue curve developed. Mean stress effects were included due to the presence of denting and applied loadings. The results indicated that a 10% reduction in stability ratio is needed (considering the range of possible initiation stress amplitudes) to reduce the fatigue usage per year to less than 0.021 for a tube similar to Row 9 Column 51 at North Anna Unit 1.

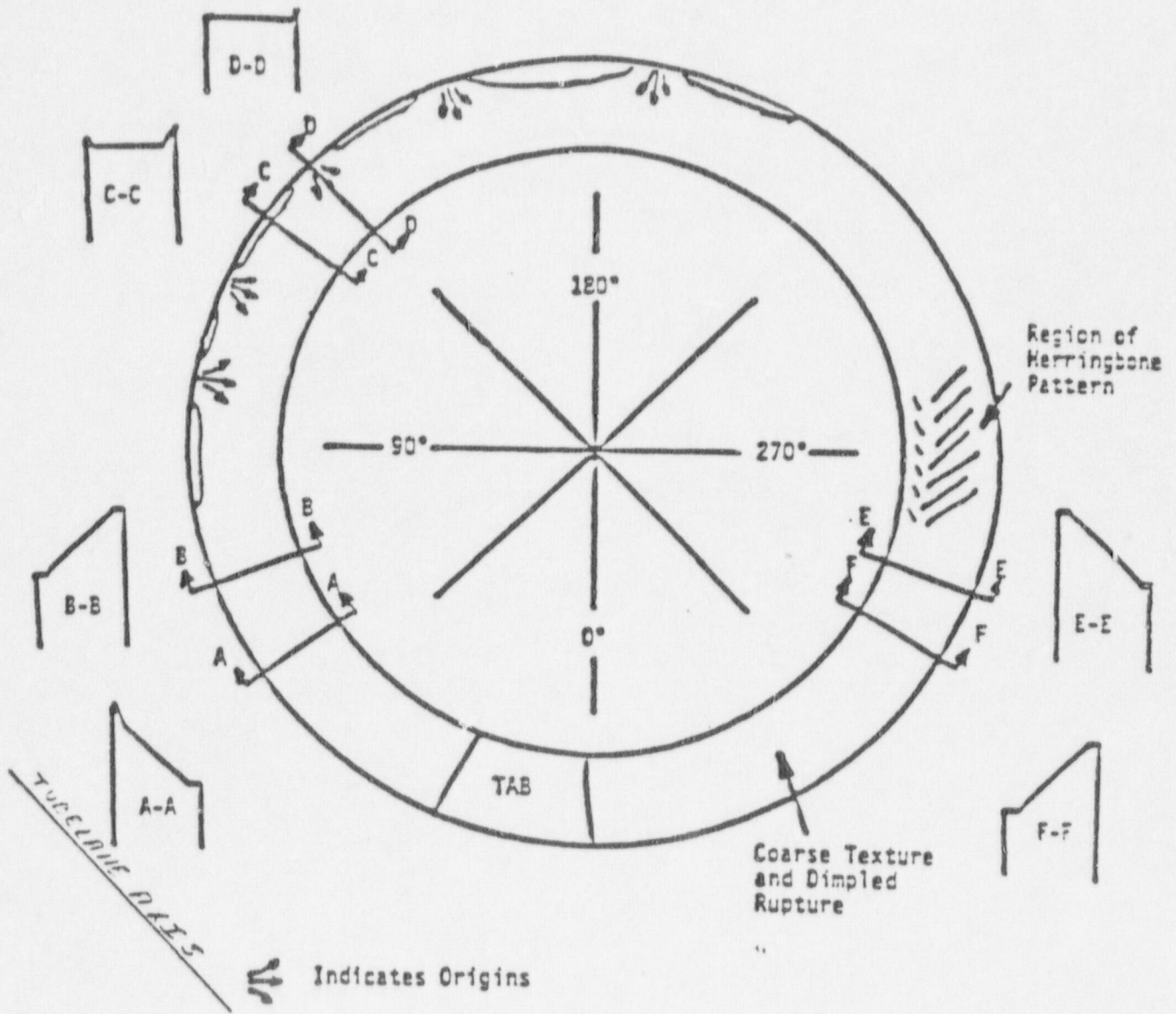
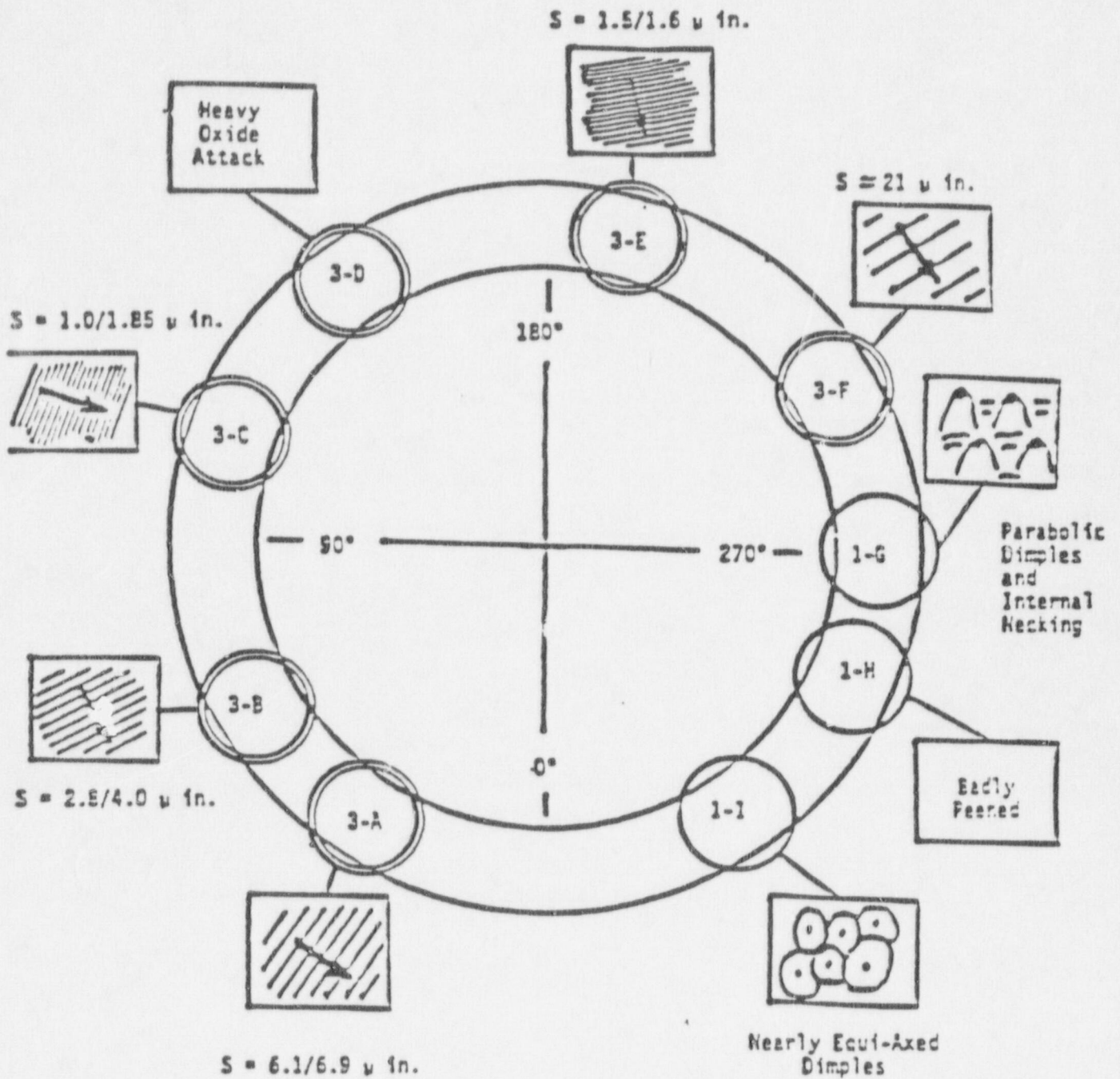


Figure 3-1 Approximate Mapping of Fracture Surface of Tube R9C51, S/G "C" Cold Leg, North Anna Unit 1



Note: Arrows Indicate Direction of Fracture Propagation

Figure 3-2 Schematic Representation of Features Observed During TEM Fractographic Examination of Fracture Surface of Tube R9C51, S/G "C" Cold Leg, North Anna Unit 1

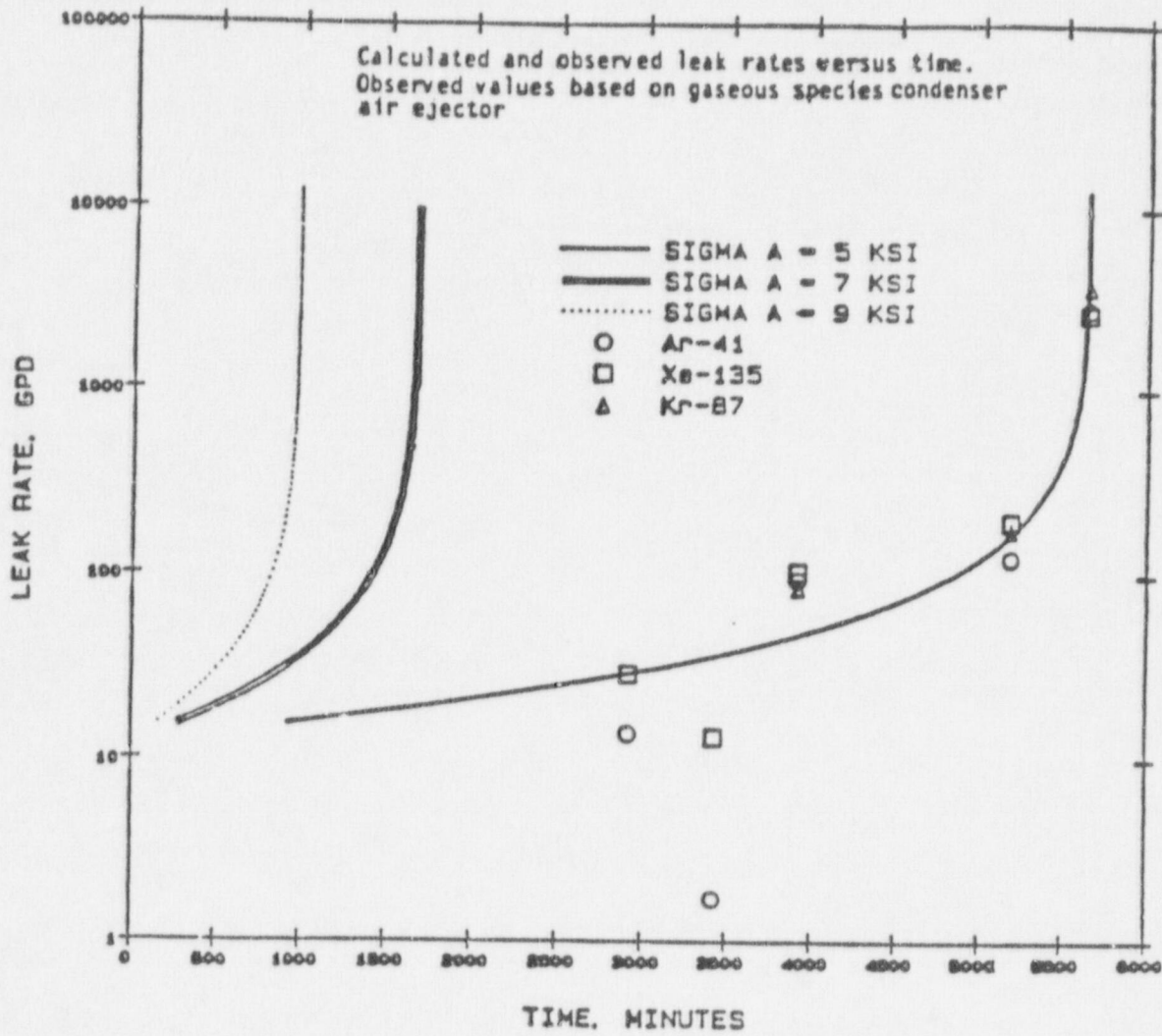


Figure 3-3 Calculated and Observed Leak Rates Versus Time

4.0 CRITERIA FOR FATIGUE ASSESSMENT

The evaluation method and acceptance criteria are based on a relative comparison with the Row 9 Column 51 tube of Steam Generator C, North Anna Unit 1. This approach is necessary because (1) methods for direct analytical prediction of actual stability ratios incorporate greater uncertainties than a relative ratio method, and (2) the stress amplitude (or displacement) associated with a specific value of stability ratio can only be estimated by the analysis of North Anna Unit 1. For these reasons, the North Anna Unit 1 tubing evaluation was done on a relative basis to Row 9 Column 51 and a 10% reduction in stability ratio criteria was established to demonstrate that tubes left in service would be expected to have sufficiently low vibration stress to preclude future fatigue rupture events.

To accomplish the necessary relative assessment of Beaver Valley Unit 2 tubing to Row 9 Column 51 of North Anna Unit 1, several criteria are utilized. First, stability ratios are calculated for the Beaver Valley Unit 2 steam generators based on flow fields predicted by 3-D thermal hydraulic models and ratioed to the stability ratio for Row 9 Column 51 at North Anna Unit 1 based on a flow field obtained with a 3-D thermal hydraulic model with the same degree of refinement. These ratios of stability ratio (called relative stability ratios) for each potentially unsupported U-bend in the Beaver Valley Unit 2 steam generators should be equivalent to ≤ 0.9 of R9C51, North Anna 1 (meeting the 10% reduction in stability ratio criteria). This provides the first level of screening of susceptible tubes incorporating all tube geometry and flow field differences in the tube dynamic evaluation. It has the inherent assumption, however, that each tube has the same local, high flow condition present at Row 9 Column 51, North Anna Unit 1. To account for these differences, flow peaking factors can be incorporated in the relative stability ratios and the relative stress ratios.

The next step is to obtain stress ratios, the ratio of stress in the Beaver Valley Unit 2 tube of interest to the stress in Row 9 Column 51, North Anna Unit 1, and after incorporating the requirement that the relative stability ratio to Row 9 Column 51 (R9C51) for the tube of interest is equivalent to ≤ 0.9 , require the stress ratio to be ≤ 1.0 . The stress ratio incorporates the tube geometry differences with R9C51 in relation to the stress calculation and also incorporates the ratio of flow peaking factor for the tube of interest to the flow peaking factor for R9C51 (flow peaking factor is defined in Section 4.2). This should provide that all tubes meeting this criteria have stress amplitudes equivalent to ≤ 4.0 ksi.

Finally, the cumulative fatigue usage for plant operation to date and for continued operation with the same operating parameters is evaluated. A fatigue usage of ≤ 1.0 may not be satisfied by meeting the stress ratio criteria using the reference operating cycle evaluation since the reference cycle does not necessarily represent the exact duty cycle to date. Therefore, the time history of operation is evaluated on a normalized basis and used together with the stress ratio to obtain a stress amplitude history. This permits the calculation of current and future fatigue usage for comparison to 1.0.

4.1 Stability Ratio Reduction Criteria

For fluidelastic evaluation, stability ratios are determined for specific configurations of a tube. These stability ratios represent a measure of the potential for flow-induced tube vibration during service. Values greater than unity (1.0) indicate instability (see Section 5.1).

Motions developed by a tube in the fluidelastically unstable mode are quite large in comparison to the other known mechanisms. The maximum modal displacement (at the apex of the tube) is linearly related to the bending stress in the tube just above the cold leg top tube support plate. This relationship applies to any vibration in that mode. Thus, it is possible for an unstable, fixed boundary condition tube to deflect an amount in the U-bend which will produce fatigue inducing stresses.

The major features of the fluidelastic mechanism are illustrated in Figure 4-1. This figure shows the displacement response (LOG D) of a tube as a function of stability ratio (LOG SR). A straight-line plot displayed on log-log coordinates implies a relation of the form $y = A(x)^n$, where A is a constant, x is the independent variable, n is the exponent (or power to which x is raised), and y is the dependent variable. Taking logs of both sides of this equation leads to the slope-intercept form of a straight-line equation in log form, $\log y = c + n \log x$, where $c = \log A$ and represents the intercept and n is the slope. In our case the independent variable x is the stability ratio SR, and the dependent variable y is tube (fluidelastic instability induced) displacement response D, and the slope n is renamed s.

From experimental results, it is known that the turbulence response curve (on log-log coordinates) has a slope of approximately $[]^{a,b,c}$. Test results also show that the slope for the fluidelastic response depends somewhat on the instability displacement (response amplitude). It has been shown by tests that a slope of $[]^{a,b,c}$ is a range of values corresponding to displacement amplitudes in the range of $[]^{a,c}$, whereas below $[]^{a,c}$ are conservative values.

The reduction in response obtained from a stability ratio reduction can be expressed by the following equation:

$$\left[\frac{D_2}{D_1} \right]^{a,c} = \left(\frac{SR_2}{SR_1} \right)^s$$

where D_1 and SR_1 are the known values at the point corresponding to point 1 of Figure 4-1 and D_2 and SR_2 are values corresponding to any point lower on this curve. Therefore, this equation can be used to determine the reduction in displacement response for any given reduction in stability ratio.

This equation shows that there is benefit derived from even a very small percentage change in the stability ratio. It is this reduction in displacement for a quite small reduction in stability ratio that formed the basis for demonstrating that a 10% reduction in stability ratio would be sufficient to prevent Row 9 Column 51 from rupturing by fatigue.

The fatigue curve developed for the North Anna Unit 1 tube at R9C51 is from [

] ^{a,c}. Thus,

$$\left[\dots \right]^{a,c}$$

where, σ_a is the equivalent stress amplitude to σ_a that accounts for a maximum stress of σ_y , the yield strength. The -3 sigma curve with mean stress effects is shown in Figure 4-2 and is compared to the ASME Code Design Fatigue Curve for Inconel 600 with the maximum effect of mean stress. The curve utilized in this evaluation is clearly well below the code curve reflecting the effect of an AVT environment on fatigue and [

] ^{a,c} for accounting for mean stress that applies to materials in a corrosive environment.

Two other mean stress models were investigated for the appropriateness of their use in providing a reasonable agreement with the expected range of initiating stress amplitudes. These were the [^{a,c}] shown in Figure 4-3. With a [

] ^{a,c}, the [

] ^{a,c}.

The assessment of the benefit of a reduction in stability ratio begins with the relationship between stability ratio and deflection. For a specific tube geometry, the displacement change is directly proportional to change in stress so that stress has the same relationship with stability ratio,

$$\left[\frac{\sigma}{SR} \right]^{a,c}$$

The slope in this equation can range from []^{a,c} on a log scale depending on the amplitude of displacement. Knowing the stress resulting from a change in stability ratio from SR₁ to SR₂, the cycles to failure at the stress amplitude was obtained from the fatigue curve. A fatigue usage per year was then determined assuming continuous cycling at the natural frequency of the tube. The initial stress was determined to be in the range of 4.0 to 10.0 ksi by the fractography analysis.

It was further developed that the maximum initiating stress amplitude was not more than 9.5 ksi. This was based on [

] ^{a,c}. The corresponding

stress level is 5.6 ksi.

The maximum stress, 9.5 ksi, would be reduced to [] ^{a,c} with a 10% reduction in stability ratio and would have a future fatigue usage of [] ^{a,c} per year at 75% availability, Figure 4-4. The minimum stress, 5.6 ksi, would be reduced to [] ^{a,c} ksi with a 5% reduction in stability ratio and would have future fatigue usage of [] ^{a,c} per year, Figure 4-5. In addition, if a tube were already cracked, the crack could be as large as [] ^{a,c} inch in length and thru-wall and would not propagate if the stress amplitudes are reduced to ≤ 4.0 ksi.

Subsequent to the return to power evaluation for North Anna Unit 1, the time history of operation was evaluated on a normalized basis to the last cycle, confirming the conservatism of 9.5 ksi. [

] ^{a,c} for R9C51, North Anna Unit 1, Steam Generator C, and that the major portion of the fatigue usage came in the second, third and fourth cycles. The first cycle was conservatively omitted, since denting is assumed, for purposes of this analysis, to have occurred during that first cycle. Based on this evaluation, the tube fatigue probably occurred over most of the operating history of North Anna Unit 1.

A similar calculation can be performed for the time history of operation assuming that [

] ^{a,c}.
On this basis, the effect of a 10% reduction in stability ratio is to reduce the stress amplitude to 4.0 ksi and results in a future fatigue usage of [^{a,c}.

Other combinations of alternating stress and mean stress were evaluated with -3 sigma and -2 sigma fatigue curves to demonstrate the conservatism of the 10% reduction in stability ratio. Table 4-1 presents the results of the cases analyzed clearly demonstrating that the 10% reduction in stability ratio combined with a -3 sigma fatigue curve and with maximum mean stress effects is conservative. Any higher fatigue curve whether through mean stress, mean stress model, or probability, results in greater benefit for the same reduction in stability ratio. Further, for any of these higher curves, a smaller reduction in stability ratio than 10% would result in the same benefit. In addition, there is a large benefit in terms of fatigue usage for relatively small changes in the fatigue curve.

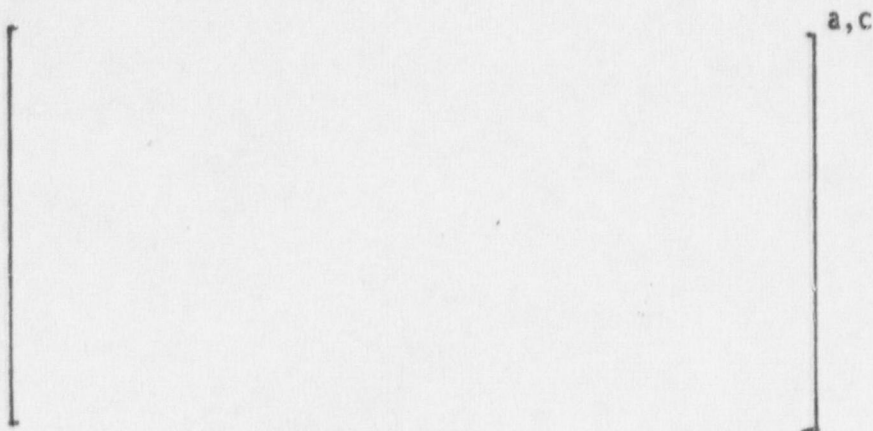
4.2 Local Flow Peaking Considerations

Local flow peaking is a factor on stability ratio that incorporates the effect on local flow velocity, density and void fraction due to non-uniform AVB insertion depths. The flow peaking factor is applied directly to the stability ratio obtained from thermal-hydraulic analysis that does not account for these local geometry effects. Being a direct factor on stability ratio, a small percentage increase can result in a significant change in the prediction of tube response.

Since the evaluation of Beaver Valley Unit 2 tubing is relative to R9C51, North Anna Unit 1, the flow peaking factors are also applied as relative ratios, i.e., a ratio of Beaver Valley Unit 2 tubing to R9C51 at North Anna Unit 1. The flow peaking relative instability is obtained by testing in the air test rig described in Section 5.4, where the peaking factor is defined as the critical velocity for R9C51 AVB pattern compared to critical velocity for a uniform AVB pattern. As explained in Section 8.0, the minimum value of $[]^{a,b,c}$ is appropriate for R9C51 of North Anna 1. The peaking factor for a tube in Beaver Valley Unit 2 tubing is therefore divided by $[]^{a,b,c}$ and the resulting relative flow peaking is multiplied times the relative stability ratio based on ATHOS results. If the peaking factor is 1.0, the relative flow peaking is $[]^{a,b,c}$.

As a further demonstration of the conservatism of $[]^{a,b,c}$ as the minimum flow peaking factor for R9C51, the stress amplitude of 7.0 ksi obtained from iterating on cumulative fatigue usage (and selected as the nominal value from fractography analysis) was used to back calculate the apparent stability ratio and then the apparent flow peaking factor. Allowing for a range of slopes of the instability curve from 10 to 30, the stability ratio is in the range of 1.1 to 1.4 and the flow peaking factor is in the range of 1.8 to 2.2. This range of flow peaking agrees with the range of flow peaking factors measured in the air tests and is considered to be the best estimate of the range of the R9C51 flow peaking factor.

The range of stability ratios, 1.1 to 1.4, is based on a value of 0.63 obtained with ATHOS results without flow peaking and with nominal damping that is a function of modal effective void fraction (MEVF). MEVF is calculated using the formula:



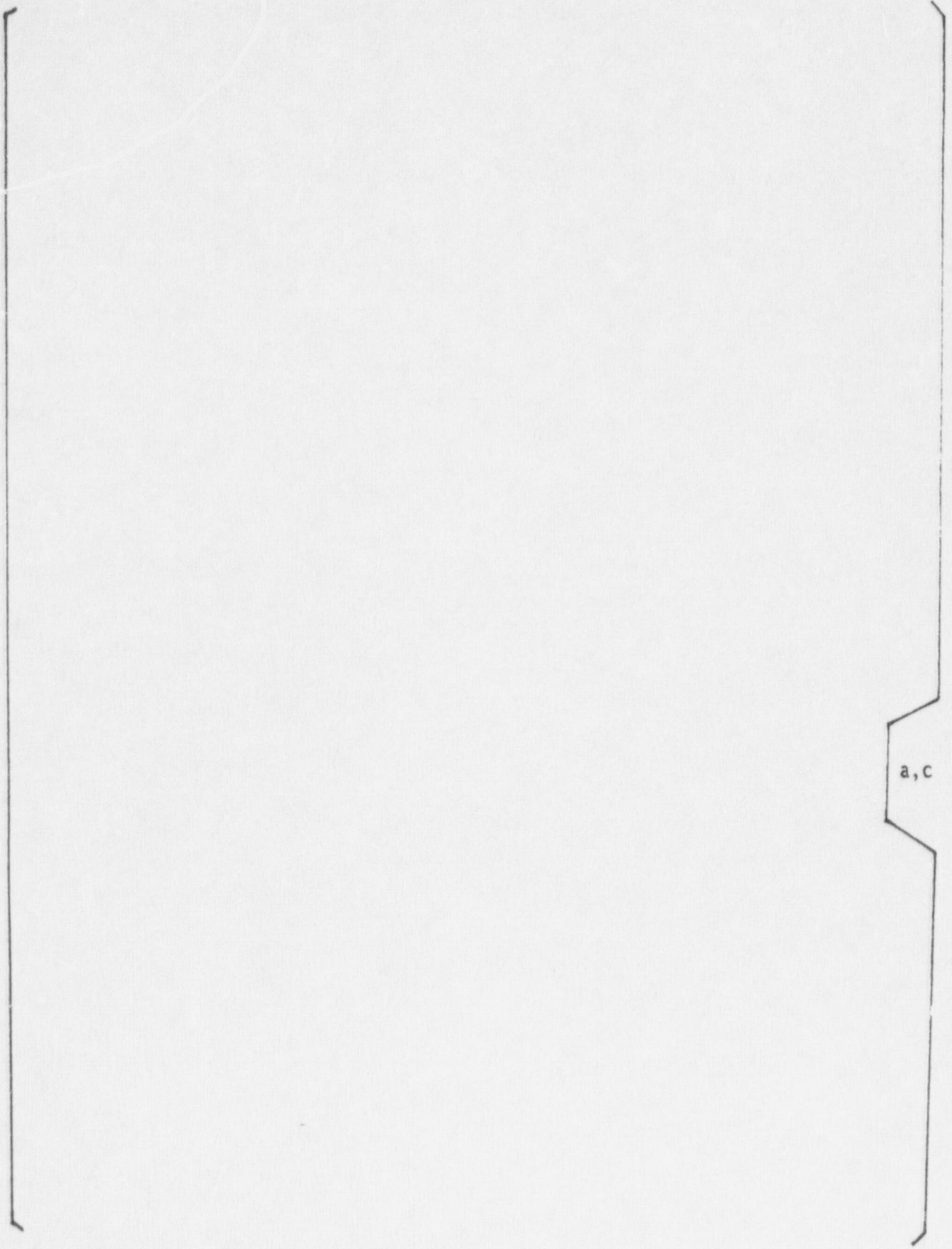
The nominal damping reflects the nominal reduction in damping that occurs with denting at the tube support plate. Therefore, a minimum damping scenario that is independent of void fraction is not considered to be credible and is not addressed in the evaluation that follows.

4.3 Stress Ratio Considerations

In Section 4.1, a 10% reduction in stability ratio was established to reduce the stress amplitude on the Row 9 Column 51 tube of North Anna Unit 1 to a level that would not have ruptured, 4.0 ksi. To apply this same criteria to another tube in the same or another steam generator, the differences in [

]a, c.

a, c



a, c

By establishing their equivalent effect on the stress amplitude that produced the tube rupture at North Anna 1, several other effects may be accounted for. These include a lower mean stress (such as for non-dented tubes), different frequency tubes from the []^{a,c,e} hertz frequency of R9C51, North Anna 1, and shorter design basis service.

In the case of lower mean stress, the stress amplitude that would have caused the failure of R9C51, North Anna 1, would have been higher. [

] ^{a,c}.

A lower or higher frequency tube would not reach a usage of 1.0 in the same length of time as the R9C51 tube due to the different frequency of cycling. The usage accumulated is proportional to the frequency and, therefore, the allowable number of cycles to reach a usage of 1.0 is inversely proportional to frequency. The equivalent number of cycles to give the usage of 1.0 for a different frequency tube [

] ^{a,c}.

For a different time basis for fatigue usage evaluation, [

] ^{a,c,e}.

Knowing the magnitude of the stress ratio allows 1) the determination of tubes that do not meet a value of ≤ 1 , and 2) the calculation of maximum stress in the acceptable tubes,

$$\left[\quad \quad \quad \right] \quad a, c$$

Having this maximum stress permits the evaluation of the maximum fatigue usage for Beaver Valley Unit 2 based on the time history expressed by normalized stability ratios for the duty cycle (see Section 7.4).

Table 4-1
 Fatigue Usage per Year Resulting
 From Stability Ratio Reduction

| SR, % REDUCTION | STRESS BASIS(1) | FATIGUE CURVE(2) | MEAN STRESS MODEL | USAGE PER YEAR |
|--------------------|--|---------------------|----------------------|-------------------|
| 5. | 9 yrs to fail [] ^{a,c} | [] | |] a, c |
| 5. | 9 yrs to fail [] ^{a,c} | | | |
| 5. | 9 yrs to fail [] ^{a,c} | | | |
| 10. | max. stress amplitude ⁽⁴⁾ [] ^{a,c} | | | |
| 10. | max. stress amplitude ⁽⁴⁾ [] ^{a,c} | | | |
| 10. | max. stress amplitude ⁽⁴⁾ [] ^{a,c} | | | |
| 10. | max. stress amplitude ⁽⁴⁾ [] ^{a,c} | | | |
| 10. | max. stress based on duty cycle ⁽⁵⁾ [] ^{a,c} | | | |

(1) This gives the basis for selection of the initiating stress amplitude and its value in ksi.

(2) S_m is the maximum stress applied with $S_m = S_{mean} + S_a$.

(3) []^{a,c}.

(4) Cycles to failure implied by this combination of stress and fatigue properties is notably less than implied by the operating history. Consequently this combination is a conservative, bounding estimate.

(5) Cycles to failure implied by the operating history requires []^{a,c} fatigue curve at the maximum stress of []^{a,c}.



Figure 4-1 Vibration Displacement vs. Stability Ratio

a, c

Figure 4-2 Fatigue Strength of Inconel 600 in AVT Water at 600°F

a, c

Figure 4-3 Fatigue Curve for Inconel 600 in AVT Water
Comparison of Mean Stress Correction Models

a, c

Figure 4-4 Modified Cumulative Fatigue Factor with 10% Reduction
in Stability Ratio for Maximum Stress Condition

a, c

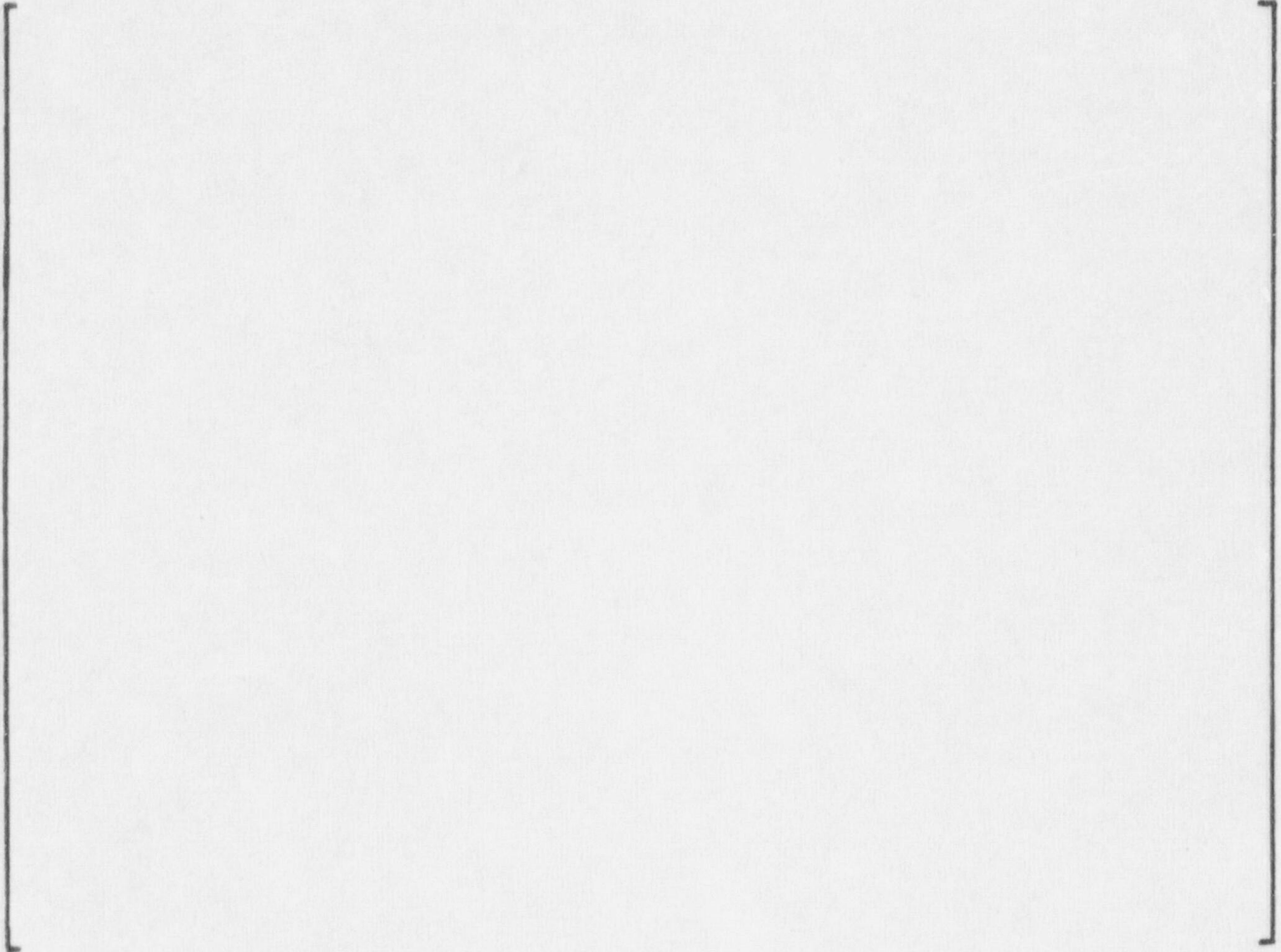


Figure 4-5 Modified Cumulative Fatigue Factor with 5% Reduction
in Stability Ratio for Minimum Stress Condition

5.0 SUPPORTING TEST DATA

This section provides a mathematical description of the fluid-elastic mechanism, which was determined to be the most likely causative mechanism for the North Anna tube rupture, as discussed in Section 3.3, to highlight the physical conditions and corresponding parameters directly related to the event and associated preventative measures. The basis for establishing the appropriate values and implications associated with these parameters are provided. Where appropriate, test results are presented.

5.1 Stability Ratio Parameters

Fluid-elastic stability ratios are obtained by evaluations for specific configurations, in terms of active tube supports, of a specific tube. These stability ratios represent a measure of the potential for tube vibration due to instability during service. Fluid-elastic stability evaluations are performed with a computer program which provides for the generation of a finite element model of the tube and tube support system. The finite element model provides the vehicle to define the mass and stiffness matrices for the tube and its support system. This information is used to determine the modal frequencies (eigenvalues) and mode shapes (eigenvectors) for the linearly supported tube being considered.

The methodology is comprised of the evaluation of the following equations:

Fluid-elastic stability ratio = $SR = U_{en}/U_c$ for mode n ,

where U_c (critical velocity) and U_{en} (effective velocity) are determined by:

$$U_c = \beta f_n D \left\{ (m_0 \delta_n) / (\rho_0 D^2) \right\}^{1/2} \quad [1]$$

and;

$$U_{en}^2 = \frac{\sum_{j=1}^N (\rho_j/\rho_0) U_j^2 \phi_{jn}^2 z_j}{\sum_{j=1}^N (m_j/m_0) \phi_{jn}^2 z_j} \quad [2]$$

where,

- D = tube outside diameter, inches
- U_{en} = effective velocity for mode n , inches/sec
- N = number of nodal points of the finite element model
= number of degrees of freedom in the out-of-plane direction
- m_j, U_j, ρ_j = mass per unit length, crossflow velocity and fluid density at node j , respectively
- ρ_0, m_0 = reference density and a reference mass per unit length, respectively (any representative values)
- δ_n = logarithmic decrement (damping)
- ϕ_{jn} = normalized displacement at node j in the n th mode of vibration
- z_j = average of distances between node j to $j-1$, and j to $J+1$
- β = an experimentally correlated stability constant

Substitution of Equations [1] and [2] into the expression which defines stability ratio, and cancellation of like terms, leads to an expression in fundamental terms (without the arbitrary reference mass and density parameters). From this resulting expression, it is seen that the stability ratio is directly related to the flow field in terms of the secondary fluid velocity times square-root-density distribution (over the tube mode shape), and inversely related to the square root of the mass distribution, square root of modal damping, tube modal frequency, and the stability constant (Eq. 5a).

The uncertainty in each of these parameters is addressed in a conceptual manner in Figure 5-1. The remainder of this section (Section 5.0) provides a discussion, and, where appropriate, the experimental bases to quantitatively establish the uncertainty associated with each of these parameters. In

A summary of the test bases and qualifications of the beta values used for these assessments is provided by Figure 5-2. The lowest measured beta for tubes without AVBs was a value of []^{a,b,c}. This value is used for the beta parameter in all stability ratio evaluations addressed in this Report (see also "Average Flow Field" subsection below).

Mass Distribution

The mass distribution parameter is based on known information on the tube and primary and secondary fluid physical properties. The total mass per unit length is comprised of that due to the tube, the internal (primary) fluid, and the external (secondary) fluid (hydrodynamic mass). Data in Reference 5-2 suggests that at operating void fractions [

] ^{a,c}.

Tube Damping

Test data are available to define tube damping for clamped (fixed) tube supports, appropriate to dented tube conditions, in steam/water flow conditions. Prototypic U-bend testing has been performed under conditions leading to pinned supports. The data of Axisa in Figure 5-4 provides the principal data for clamped tube conditions in steam/water. This data was obtained for cross flow over straight tubes. Uncertainties are not defined for the data from these tests. Detailed tube damping data used in support of the stability ratio evaluations addressed in this report are provided in Section 5.2, below.

Flow Field - Velocity Times Square-Root-Density Distribution

Average and U-bend-local flow field uncertainties are addressed independently in the following.

Average Flow Field

Uncertainties in the average flow field parameters, obtained from ATHOS analyses, coupled with stability constant and frequency, are essentially the same for units with dented or non-dented top support plates. If the errors associated with these uncertainties were large, similar instabilities would be expected in the non-dented units with resulting wear at either the top support plate or inner row AVBs. Significant tube wear has not been observed in inner row tubes in operating steam generators without denting. Thus, an uncertainty estimate of about []^{a,c} for the combined effects of average flow field, stability constant and frequency appears to be reasonable. To further minimize the impact of these uncertainties, the Beaver Valley Unit 2 tubes are evaluated on a relative basis, so that constant error factors are essentially eliminated. Thus, the uncertainties associated with the average velocity times square-root-density (combined) parameter are not expected to be significant.

U-Bend Local Flow Field

Non-uniform AVB insertion depths have been shown to have effects on stability ratios. Flow peaking, brought about by the "channeling" effects of non-uniform AVBs, leads to a local perturbation in the velocity times square-root-density parameter at the apex of the tube where it will have the largest effect (because the apex is where the largest vibration displacements occur). Detailed local flow field data used in support of the stability ratio evaluations addressed in this report are provided in Section 5.2, below.

Overall Uncertainties Assessment

Based on the above discussions, and the data provided in the following sections, it is concluded that local flow peaking is likely to have contributed significantly to the instability and associated increased vibration amplitude for the failed North Anna tube. Ratios of stresses and stability ratios relative to the North Anna tube, R9C51, are utilized in this report to minimize uncertainties in the evaluations associated with instability constants, local flow field effects and tube damping.

5.2 Tube Damping Data

The damping ratio depends on several aspects of the physical system. Two primary determinants of damping are the support conditions and the flow field. It has been shown that tube support conditions (pinned vs clamped) affect the damping ratio significantly. Further, it is affected by the flow conditions, i.e., single-phase or two-phase flow. These effects are discussed below in more detail.

Reference (5-1) indicates that the damping ratio in two phase flow is a sum of contributions from structural, viscous, flow-dependent, and two-phase damping. The structural damping will be equal to the measured damping in air. However, in two-phase flow, the damping ratio increases significantly and is dependent on the void fraction or quality. It can be shown that the damping contribution from viscous effects are very small.

Damping ratios for tubes in air and in air-water flows have been measured and reported by various authors. However, the results from air-water flow are poor representations of the actual conditions in a steam generator (steam-water flow at high pressure). Therefore, where available, results from prototypic steam-water flow conditions should be used. Fortunately, within the past few years test data on tube vibration under steam-water flow has been developed for both pinned and clamped tube support conditions.

Two sources of data are particularly noteworthy and are used here. The first is a large body of recent, as yet unpublished data from high pressure steam-water tests conducted by Mitsubishi Heavy Industries (MHI). These data were gathered under pinned tube support conditions. The second is comprised of the results from tests sponsored by the Electric Power Research Institute (EPRI) and reported in References (5-2) and (5-3).

The damping ratio results from the above tests are plotted in Figure 5-4 as a function of void fraction. It is important to note that the void fraction is determined on the basis of [] ^{a,c}

(Reference (5-4)). The upper curve in the figure is for pinned support conditions. This curve represents a fit to a large number of data points not shown in the figure. The points on the curve are only plotting aids, rather than specific test results.

The lower curve pertains to the clamped support condition, obtained from Reference (5-3). Void fraction has been recalculated on the basis of slip flow. It may be noted that there is a significant difference in the damping ratios under the pinned and the clamped support conditions. Damping is much larger for pinned supports at all void fractions. Denting of the tubes at the top support plate effectively clamps the tubes at that location. Therefore, the clamped tube support curve is used in the current evaluation to include the effect of denting at the top tube support plate.

The Reference 5-3 data as reported show a damping value of 0.5% at 100% void fraction. The 100% void fraction condition has no two phase damping and is considered to be affected principally by mechanical or structural damping. Westinghouse tests of clamped tube vibration in air has shown that the mechanical damping is only []^{a,c} rather than the 0.5% reported in Reference (5-3). Therefore the lower curve in Figure 5-4 is the Reference (5-3) data with all damping values reduced by []^{a,c}.

5.3 Tube Vibration Amplitudes With Single-Sided AVB Support

A series of wind tunnel tests were conducted to investigate the effects of tube/AVB eccentricity on the vibration amplitudes caused by fluidelastic vibration.

[

]a,c. Prior test results obtained during the past year using this apparatus have demonstrated that the fluidelastic vibration characteristics observed in the tests performed with the cantilever tube apparatus are in good agreement with corresponding characteristics observed in wind tunnel and steam flow tests using U-bend tube arrays. A summary of these prior results is given in Table 5-1.

An overall view of the apparatus is shown in Figure 5-5. Figure 5-6 is a top view of the apparatus. [

]a,c.

As shown in Figure 5-7, the tube vibration amplitude below a critical velocity is caused by [

]a,c.

Figure 5-7 shows the manner in which the zero-to-peak vibration amplitude, expressed as a ratio normalized to []a,c, varies when one gap remains at []a,c. For increasing velocities, up to that corresponding to a stability ratio of [

]a,c. Figure 5-8 shows typical vibration amplitude and tube/AVB impact force signals corresponding to those obtained from the tests which provided the results shown in Figure 5-7. As expected, impacting is only observed in the []a,c.

It is concluded from the above test results that, [

]a,c.

5.4 Tests to Determine the Effects on Fluidelastic Instability of Columnwise Variations in AVB Insertion Depths

This section summarizes a series of wind tunnel tests that were conducted to investigate the effects of variations in AVB configurations on the initiation of fluidelastic vibration. Each configuration is defined as a specific set of insertion depths for the individual AVBs in the vicinity of an unsupported U-bend tube.

The tests were conducted in the wind tunnel using a modified version of the cantilever tube apparatus described in Section 5.3. Figure 5-9 shows the conceptual design of the apparatus. The straight cantilever tube, [

]a,c

[

]a,c.

[

]a,c. Figure 5-11 shows the AVBs, when the side panel of the test section is removed. Also shown is the top flow screen which is [

]a,c. The AVB configurations tested are shown in Figure 5-12. Configuration 1a corresponds to tube R9C51, the failed tube at North Anna. Configuration 2a corresponds to one of the cases in which the AVBs are inserted to a uniform depth and no local velocity peaking effects are expected.

As shown in Figure 5-9, [

]a,c.

All the tubes except the instrumented tube (corresponding to Row 10) are []a,c. As discussed in Section 5.3, prior testing indicates that this situation provides a valid model. The instrumented tube []a,c as shown in Figure 5.10. Its []a,c direction vibrational motion is measured using a non-contacting transducer.

[

]a,c. The instrumented tube corresponds to a Row 10 tube as shown in Figure 5-9. However, depending on the particular AVB configuration, it can reasonably represent a tube in Rows 8 through 11. The AVB profile in the straight tube model is the average of Rows 8 and 11. The difference in profile is quite small for these bounding rows.

[

]a,c using a hot-film anemometer located as shown in Figure 5-9.

Figure 5-13 shows the rms vibration amplitude, as determined from PSD (power spectral density) measurements made using an FFT spectrum analyzer, versus flow velocity for Configuration 1a (which corresponds to tube R9C51 in North Anna). Data for three repeat tests are shown and the critical velocity is identified. The typical rapid increase in vibration amplitude when the critical velocity for fluidelastic vibration is exceeded is evident.

The main conclusions from the tests are:

1. Tube vibration below the critical velocity is relatively small, typical of turbulence-induced vibration, and increases rapidly when the critical velocity for the initiation of fluidelastic vibration is exceeded.
2. Configuration 1a (R9C51 in North Anna) has among the lowest critical velocity of all the configurations tested.
3. Configuration 1b, with a similar geometry, but slightly higher peaking factor than 1a, has been periodically to verify the consistency of the test apparatus and its calibration.

The initial test results obtained in support of the Beaver Valley Unit 2 1 evaluation are summarized in Table 5-2. The test data is presented as a velocity peaking ratio; a ratio of critical velocity for North Anna tube R9C51 configuration 1a, to that for each Beaver Valley Unit 2 AVB configuration evaluated.

5.5 References

a, c

Table 5-1
Wind Tunnel Tests on Cantilever Tube Model

OBJECTIVE: Investigate the effects of tube/AVB fitup on flow-induced tube vibration.

APPARATUS: Array of cantilevered tubes with end supports [

]a,c.

MEASUREMENTS: Tube vibration amplitude and tube/AVB impact forces or preload forces.

RESULTS:

a,b,c

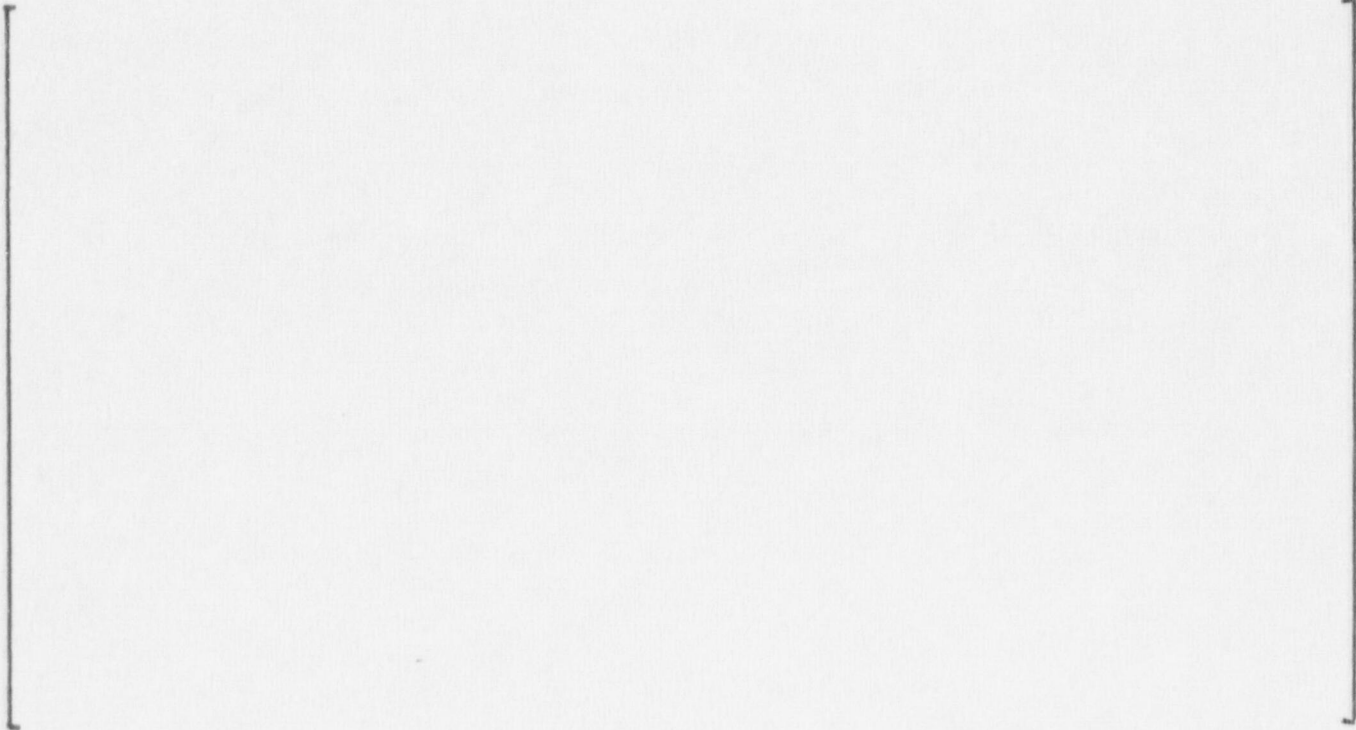


Table 5-2
 Fluidelastic Instability Velocity Peaking Ratios
 for Columnwise Variation in AVB Insertion Depths
 (BEAVER VALLEY UNIT 2)

| Type of Insertion Configuration | Peaking Ratio U_{1a}/U_n |
|--|---|
| 1a 1b 1c 1r 1v 1y 1z 2a 4a 4b 4f 4v 5a 5b 5c 5f 5g 5i 6a 6b 6c 6d 7b 7c | <div style="display: flex; align-items: center; justify-content: center;"> <div style="border-left: 1px solid black; border-right: 1px solid black; height: 300px; margin: 0 10px;"></div> a, b, c </div> |

Note: U_n is instability velocity at inlet for type n of AVB insertion configuration.

a,c

FIG e 5-1 Fluidelastic Instability Uncertainty Assessment

U-Bend Test Data

- 1) MB-3 Tests
 β values of []^{a,b,c}
- 2) MB-2 Tests
 β of []^{a,b,c}
- 3) Air Model Tests
 β of []^{a,b,c} without AVBs
Tendency for β to increase in range of []^{a,b,c}
with inactive AVBs (gaps at AVBs)
Tendency for β to decrease toward a lower bound of
[]^{a,b,c} with active AVBs

Verification of Instability Conditions

- 1) Flow conditions at critical velocity from MB-3
- 2) Measured damping for the specific tube
- 3) Calculated velocities from ATHOS 3D analysis
- 4) β determined from calculated critical values
Good agreement with reported β values
- 5) ATHOS velocity data with β of []^{a,b,c} and known damping
should not significantly underestimate instability for regions of
uniform U-bend flow

Figure 5-2 Instability Constant - β

Figure 5-3 Instability Constants, β , Obtained for Curved Tubes from Wind Tunnel Tests on the 0.214 Scale U-Bend Model

a,b,c

Figure 5-4 Damping vs. Slip Void Fraction

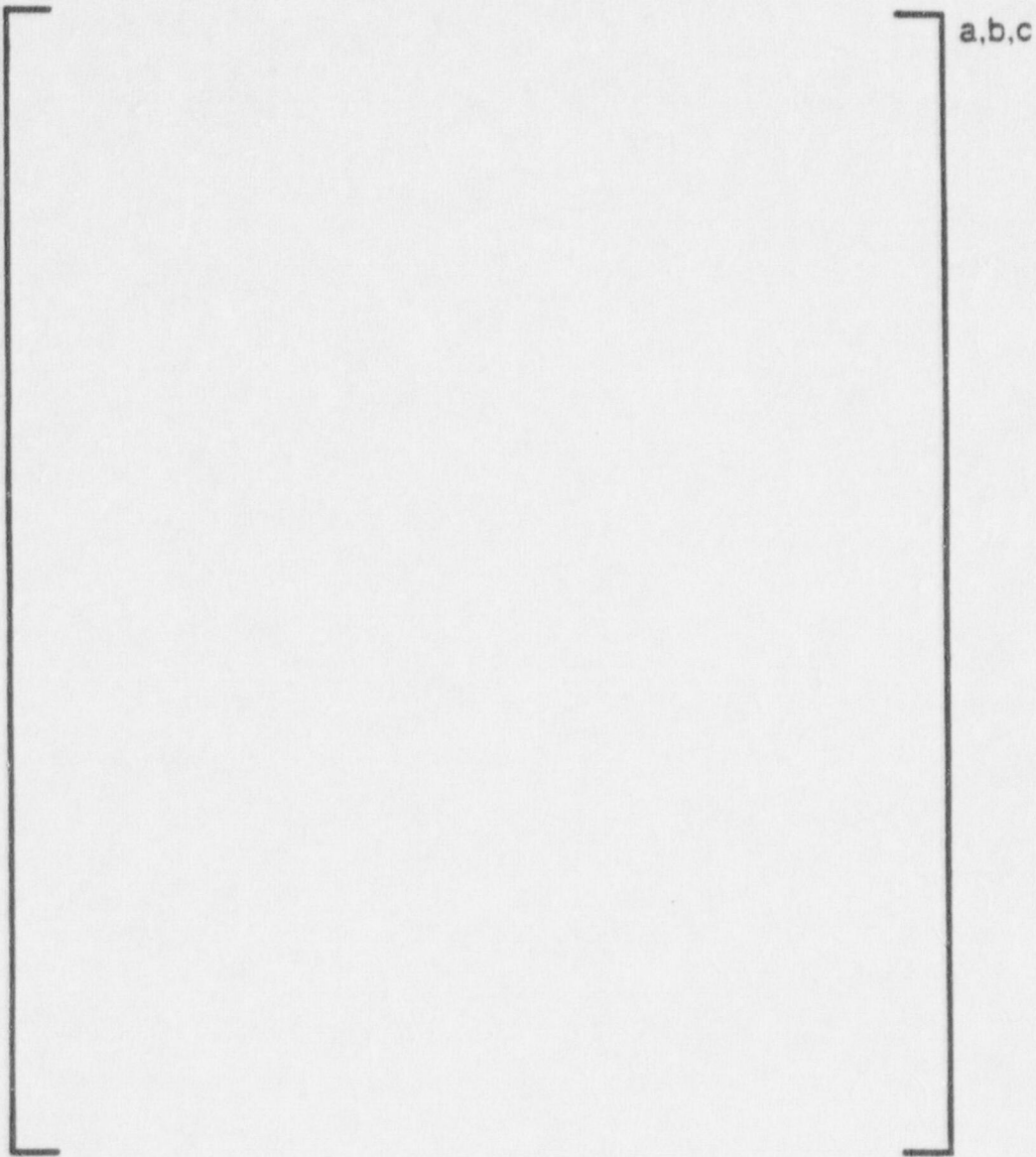


Figure 5-5 Overall View of Cantilever Tube Wind Tunnel Model



Figure 5-6 Top View of the Cantilever Tube Wind Tunnel Model

a, b.

Figure 5-7 Fluidelastic Vibration Amplitude with Non-Uniform Gaps

Figure 5-8 Typical Vibration Amplitude and Tube/AVB Impact Force Signals for Fluidelastic Vibration with Unequal Tube/AVB Gaps

Figure 5-9 Conceptual Design of the Apparatus for Determining the Effects of Fluidelastic Instability of Columnwise Variations in AVB Insertion Depths



Figure 5-10 Overall View of Wind Tunnel Test Apparatus



Figure 5-11 Side View of Wind Tunnel Apparatus with Cover Plates
Removed to Show Simulated AVBs and Top Flow Screen

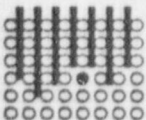
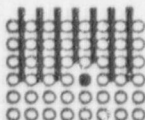
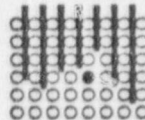
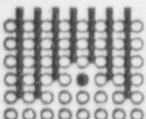
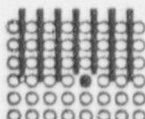
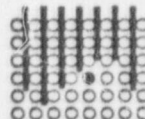
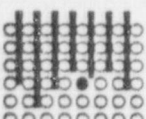
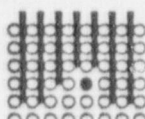
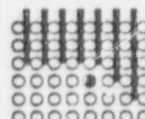
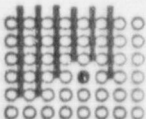
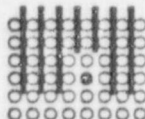
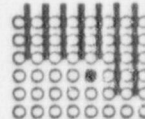
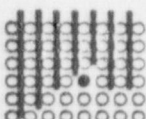
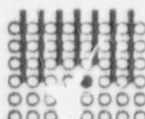
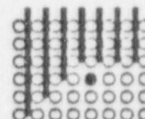
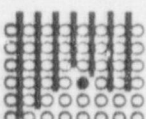
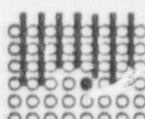
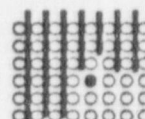
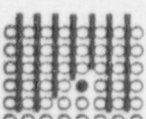
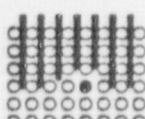
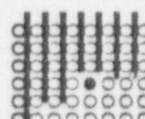
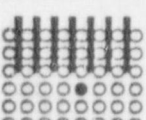
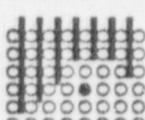
| TYPE OF AVB INSERTION | TYPE OF AVB INSERTION | TYPE OF AVB INSERTION |
|--|--|--|
| 1a  | 4a  | 5g  |
| 1b  | 4b  | 5i  |
| 1c  | 4f  | 6a  |
| 1r  | 4v  | 6b  |
| 1v  | 5a  | 6c  |
| 1y  | 5b  | 6d  |
| 1z  | 5c  | 7b  |
| 2a  | 5f  | 7c  |

Figure 5-12 AVB Configurations Tested for Beaver Valley 2

a, b, c

Figure 5-13 Typical Variation of RMS Vibration Amplitude with Flow Velocity for Configuration 1a in Figure 5-12

6.0 EDDY CURRENT DATA AND AVB POSITIONS

The EC input to the Beaver Valley Unit 2 analyses is based on EC tapes generated during the 'baseline' inspection performed in 1985:

S/G U-Bend Examination Date:

| | |
|---|-----------|
| A | Aug 1985 |
| B | Aug 1985 |
| C | Sept 1985 |

6.1 AVB Assembly Design

[

]a,c,e 'Upper' AVBs which are inserted beyond the design depth, occasionally show on the EC traces for the Row 12 tubes. Since the purpose of this analysis is to evaluate potentially unsupported tubes at or near the point of maximum AVB insertion, only the dimensions and EC data pertaining to the 'lower' AVBs are used.

6.2 Eddy Current Data for AVB Positions

The AVB insertion depths were determined on the basis of interpretation of the eddy current data. To locate the AVBs, the ECT data traces were searched for the characteristic peaks seen in the signals, which indicate the intersection of an AVB (or a tube support plate) with the tube (a typical signal for AVBs is shown in Figure 6.1). Since ambiguity can occur in the interpretation of the

ECT data, due to inability of ECT to differentiate at which side of a tube a "visible" AVB is located, other information must be used to assist in establishing the location of the AVBs. Consistency with the design of the AVB assembly, consistency of data for adjacent columns, and verification by projection were utilized to determine the depth of insertion which was plotted.

For Beaver Valley Unit 2 the number of AVB intersections, including zero (meaning no AVB present), was logged for each tube to indicate the presence or absence of AVBs. Figures 6-2 through 6-4 show the number of AVB signals found for each tube, and a representation of AVB insertion distance based on evaluation of the EC data. Details of AVB projection techniques based on EC data and tests are given in Section 6.2.2.

6.2.1 AVB Insertion Depths

AVB position maps for the Beaver Valley Unit 2 steam generators are given in Figures 6-2 through 6-4.

The direct observation data (the number of AVB intersections seen by the eddy current probe) are the principal basis for determining the AVB positions. [

] ^{a,c} Where

the direct observations were ambiguous or there is a conflict between observations and projections, the more conservative data are used to determine the AVB positions. Since 'direct observation' gives a 'yes - no' type of answer, the projection method is used to 'interpolate' AVB insertion depths between rows of tubes. The visual images thus produced are more easily understood when fluid flow peaking situations are evaluated. Greater conservatism is generally interpreted as the AVB being less inserted although consideration must also be given to the resulting flow peaking factors for tubes 'upstream' of an AVB.

ECT data, due to inability of ECT to differentiate at which side of a tube a "visible" AVB is located, other information must be used to assist in establishing the location of the AVBs. Consistency with the design of the AVB assembly, consistency of data for adjacent columns, and verification by projection were utilized to determine the depth of insertion which was plotted.

For Beaver Valley Unit 2 the number of AVB intersections, including zero (meaning no AVB present), was logged for each tube to indicate the presence or absence of AVBs. Figures 6-2 through 6-4 show the number of AVB signals found for each tube, and a representation of AVB insertion distance based on evaluation of the EC data. Details of AVB projection techniques based on EC data and tests are given in Section 6.2.3.

6.2.1 AVB Insertion Depths

AVB position maps for the Beaver Valley Unit 2 steam generators are given in Figures 6-2 through 6-4.

The direct observation data (the number of AVB intersections seen by the eddy current probe) are the principal basis for determining the AVB positions. Where the direct observations were ambiguous or there is a conflict between observations and projections, the more conservative data are used to determine the AVB positions. Since 'direct observation' gives a 'yes - no' type of answer, the projection method is used to 'interpolate' AVB insertion depths between rows of tubes. The visual images thus produced are more easily understood when fluid flow peaking situations are evaluated. Greater conservatism is generally interpreted as the AVB being less inserted although consideration must also be given to the resulting flow peaking factors for tubes 'upstream' of an AVB.

6.2.2 AVB Projection

The projection technique is useful where noisy or spurious ECT signals prevent direct observation of the AVBs and where data is unavailable due to a tube having been plugged. [

]a,c.

In the case where the AVB characteristic signals can not be confidently determined due to a noisy signal or pre-existing plugged tubes, data for locating the AVBs is provided from [

]a,c.

[

]a,c

6.3 Tube Denting at Top Tube Support Plate

Because of the AVB geometries involved and the desire to obtain 3 rows of 'projection' data where possible, the Beaver Valley Unit 2 evaluation covers Rows 8 through 12 as a minimum. EC data was evaluated as far out as Row 15 (though not plotted) to confirm projection of AVBs for Row 11 tubes with 'zero' and '1' signals found in SG's B and C. Subsequent to identifying the AVB signals, eddy current data were examined to evaluate the incidence of corrosion and/or denting at the top tube support plate. In this evaluation, the EC tapes were examined to determine the condition of the tube/TSP interface for potentially unsupported tubes in locations which could be susceptible to flow peaking. At the time the analysis was performed, Beaver Valley Unit 2 was operating on its first fuel loading, and no EC data was available except for the 'baseline' data taken in 1985. As would be expected, analysis of that data indicates that no corrosion products were present at any of the tube/TSP interfaces. Because the tube vibration analyses are based on the conservative assumption that all tubes in the area of interest are structurally 'fixed' in the TSP holes, as if by denting or corrosion, the results of this phase of the examination, but do not influence the disposition of the tubes found to be susceptible to fatigue.

6.4 AVB Map Interpretations

The Beaver Valley Unit 2 SG AVBs, have a nominal design insertion depth intended to support as far inward as the Row 11 tubes. Evaluation of the EC data indicates that in the area of interest (Row 12 through Row 8) between Columns 3 and 92, all of the Row 12 tubes, all but 5 Row 11 tubes, all but 13 Row 10 tubes, and all but 73 Row 9 tubes were supported in the three SGs.

SG-A

The AVB map for SG-A is given in Figure 6-2. A listing of unsupported tubes is given in Table 6-1. All of the Row 12 and Row 11 tubes are supported by AVBs. Two Row 10 tubes, and 15 Row 9 tubes are not supported. The highest flow peaking factors for this SG (see Sec. 8 and 9 of this report) were found

in tube locations R9C60, C83 and C84; and R8C24, C35, and C60. Peaking ratio, stability ratio, and stress ratio modifications reduce the stress ratios for all of these values to less than unity. (See Table 9.2)

SG-B

The AVB map for SG-B is given in Figure 6-3. A listing of unsupported tubes is given in Table 6.1. All of the Row 12 tubes are supported by AVBs. Four Row 11, Seven Row 10 and 20 Row 9 tubes are not supported. The highest flow peaking factors for this SG are at R11C5 but are not sufficiently high that plugging is recommended. The remaining unsupported Row 9, 10, and 11 tubes do not have significant, flow peaking factors. Peaking ratio, stability ratio, and stress ratio modifications reduce the stress ratios for all of those tubes to less than below unity. (See Table 9-2)

SG-C

The AVB map for SG-C is given in Figure 6-4. A listing of unsupported tubes is given in Table 6.1. All of the Row 12 tubes are supported by AVBs. One Row 11, four Row 10, and 38 Row 9 tubes are not supported. The highest flow peaking factors for this SG were found at R11C4, R10C4, R10C5, R9C33, R9C34, R9C35 and R9C88. The two tubes at locations R11C4 and R9C33 exceed the limiting stress ratio criteria, lending to the recommendation that they should be plugged. Peaking ratio, stability ratio, and stress ratio modifications reduced all of the remaining values to less than below unity. (See Table 9-2)

Table 6.1
Beaver Valley Unit 2
Summary Listing of Unsupported Tubes

Beaver Valley Unit 2 Steam Generator 'A'

| | |
|--------|--|
| Row 12 | Row 12 has no unsupported tubes |
| Row 11 | Row 11 has no unsupported tubes |
| Row 10 | Columns 2, and 3 are unsupported |
| Row 9 | Columns 2 thru 14, 83, and 84 are unsupported |
| Row 8 | Columns 2 thru 18, 24, 35, 39 thru 56, 60, 79 thru 84 and 87 thru 90 are unsupported |

Beaver Valley Unit 2 Steam Generator 'B'

| | |
|--------|---|
| Row 12 | Row 12 has no unsupported tubes |
| Row 11 | Columns 2 thru 5 are unsupported |
| Row 10 | Columns 2 thru 5, and 91 thru 93 are unsupported |
| Row 9 | Columns 2 thru 5, 41 thru 50, 53, 60, and 90 thru 93 are unsupported |
| Row 8 | Columns 2 thru 6, 9 thru 15, 34, 38 thru 57, 60, 61, and 90 thru 93 are unsupported |

Beaver Valley Unit 2 Steam Generator 'C'

| | |
|--------|--|
| Row 12 | Column 12 has no unsupported tubes |
| Row 11 | Column 4 is unsupported |
| Row 10 | Columns 2 thru 5 are unsupported |
| Row 9 | Columns 2 thru 12, 33 thru 35, 42, 43, 46 thru 55, 60, 79 thru 84, and 88 thru 93 are unsupported |
| Row 8 | Columns 2 thru 18, 25 thru 27, 33 thru 35, 38 thru 56, 60, 61, 69, thru 72, 77 thru 85, and 88 thru 93 are unsupported |

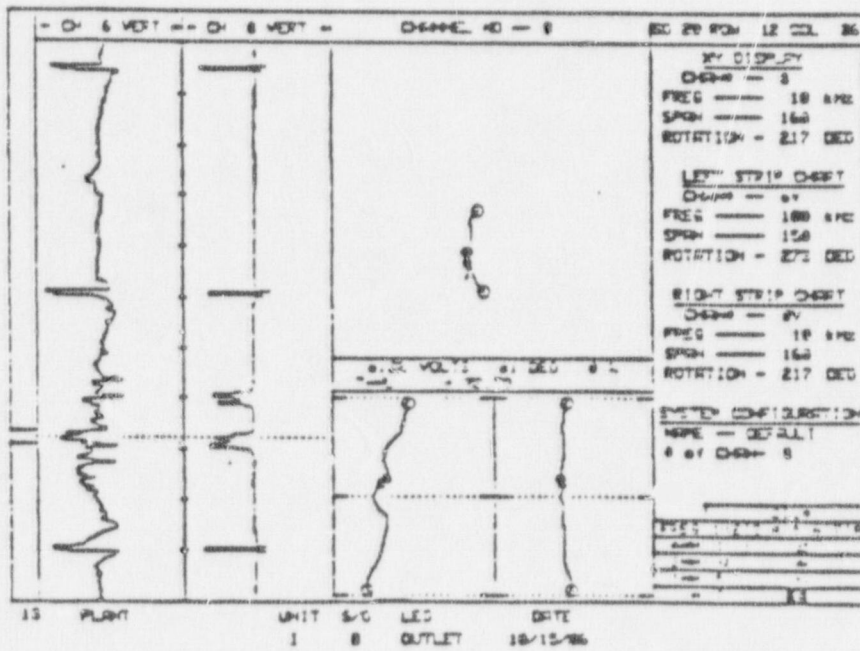
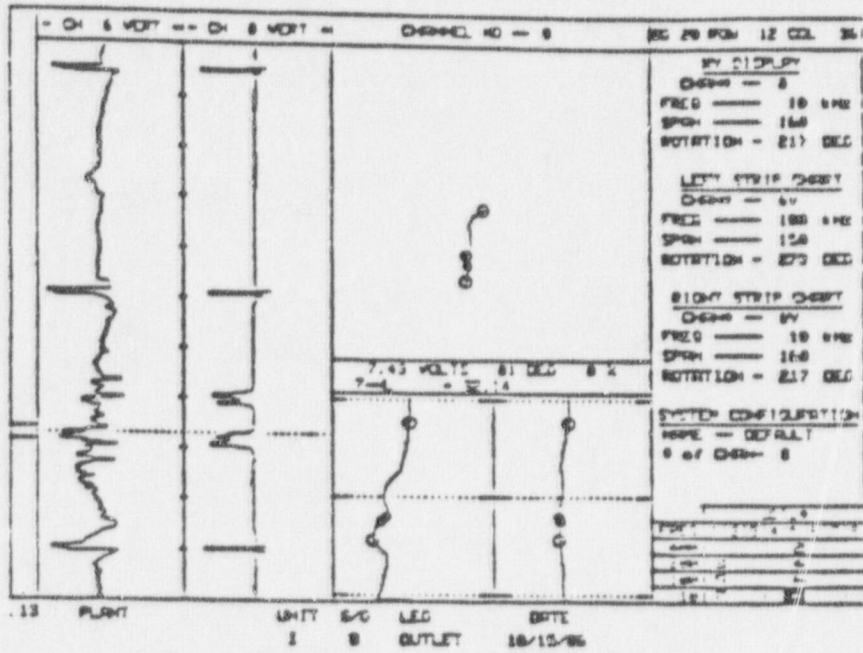


Figure 6-1 AVB Insertion Depth Confirmation

7.0 THERMAL AND HYDRAULIC ANALYSIS

This section presents the results of a thermal and hydraulic analysis of the flow field on the secondary side of the steam generator using the 3D ATHOS computer code, Reference (7-1). The major results of the analysis are the water/steam velocity components, density, void fraction, and the primary and secondary fluid and tube wall temperatures. The distributions of the tube gap velocity and density along a given tube were obtained by reducing the ATHOS results. The ATHOS distributions used in the Beaver Valley Unit 2 analysis are based on recent operating conditions at full power.

In the following subsections, the operating condition data for Beaver Valley Unit 2 is presented along with the full power conditions used in the 3D tube bundle study. A description of the ATHOS model and some sample results are included in the next two sections. The final section describes an analysis of the operating history data for Beaver Valley Unit 2. This analysis defines a parameter termed the normalized stability ratio which provides a relative indication of the effect of past operation on the plant's fluidelastic stability ratio.

7.1 Beaver Valley Unit 2 Steam Generator Operating Conditions

Recent steam generator operating condition data for Beaver Valley Unit 2 was provided by Duquesne Light. These same data are also applicable to operation throughout the first fuel cycle. The data reported for operation at 97.8% of full power were:

1. Recent Operating Parameters for Beaver Valley Unit 2
 - a. Steam Pressure - 815 psia
 - b. Feedwater Temperature and Flow rates - 437°F; 3.8×10^6 lbs/hr
 - c. Primary Inlet and Outlet Temperatures - $T_{in} = 610^\circ\text{F}$, $T_{out} = 542^\circ\text{F}$
 - d. NSSS Thermal Load - 8.8771×10^9 Btu/hr (97.8%)
 - e. Water Level - 44% of Narrow Range Span

Rather than using these supplied conditions at 97.8% of full power, the input to the ATHOS 3D calculation was conservatively based on operation at full power. Basing the analysis on this higher power condition will result in conservative stability ratios since the steam flow is higher (higher loading) and steam pressure is lower (more voids in the bundle and less damping).

Calculations were completed using the Westinghouse SG performance computer code, GENF, to verify the plant data and to establish a complete list of operating conditions required for an ATHOS analysis. The GENF code determines the primary side temperatures and steam flow rate required to obtain the specified steam pressure at the given power rating. Besides confirming these parameters, the code calculates the circulation ratio which is of primary importance to the stability ratio analysis since it, together with the steam flow, establishes the total bundle flow rate and average loading on the tubes. It also provides an overall indication of the voids within the tube bundle since the bundle exit quality is inversely proportional to the circ ratio ($X_{exit} = 1/circ \text{ ratio}$). The calculated circulation ratio along with the other thermal/hydraulic parameters for the full power condition are listed in Table 7-1.

7.2 ATHOS Analysis Model

The calculation of relative stability ratios involves comparing the stability ratio calculated for one or more tubes in a given plant to the ratio calculated for the ruptured Row 9 Column 51 tube in the North Anna Series 51 steam generator. It makes use of ATHOS computed flow profiles for both tube bundles. Since the presence of AVBs in the U-bend region of a tube bundle could influence the overall flow field and/or the local flow parameters for a particular tube of interest, some discussion of the treatment of AVBs is necessary before presenting a description of the ATHOS model.

The ATHOS code does not include the capability to model the presence of the AVBs in the U-bend region. However, Westinghouse has modified the code to include the capability to model the AVBs via flow cell boundary resistance factors. Practical lower limits of cell size in the ATHOS code, however,

prevent a fine grid representation of the AVB V-bar shape which, in turn, limits the accuracy of the AVB representation. ATHOS calculations have been performed with and without AVBs in the model. Calculations of stability ratios relative to North Anna R9C51 show that the relative stability ratios for tubes near the center of the steam generator are essentially the same for models with or without AVBs. The ATHOS AVB modeling sensitivity studies with uniform insertion show some tendency for the AVB resistance effects to lower tube gap velocities near the central regions and to increase velocities near the peripheral tubes. However, the magnitude of this effect is uncertain due to the limitations in ATHOS for modeling the AVBs. Further, the global flow resistance of staggered AVB insertion would be less than that from uniform insertion. Based on the sensitivity studies using ATHOS models with and without uniformly inserted AVBs, the most reliable relative stability ratios (for actual steam generators with non-uniform AVB insertion depths) are expected using ATHOS models excluding AVBs and effects of variable AVB insertion depths. Those AVB effects are accounted for by using flow test results of actual AVB geometries. This approach has been utilized in the Beaver Valley Unit 2 analysis.

The ATHOS cylindrical coordinate system model for the Beaver Valley Unit 2 steam generator consists of 13,440 flow cells having 30 divisions in the circumferential (x-axis) direction, 14 divisions in the radial (y-axis) direction and 32 divisions in the axial (z-axis) direction. In the ATHOS analysis, the steam generator is considered to be symmetrical with respect to the diametral plane of symmetry of the tube bundle. The model therefore, consists of one-half of the hot leg and one-half of the cold leg sides of the steam generator. Figures 7-1 and 7-2 show the plan and the elevation views of the model. These two figures show the layout of the flow cells and identify locations for some of the geometric features. Included are the flow distribution baffle and tubelane blocks in the lower bundle region and tubelane flow slots in each of the seven tube support plates.

Figure 7-3 reproduces the plan view of the model but with the tube layout arrangement superimposed. This figure illustrates the locations of the tubes in the various flow cells. The fineness of the cell mesh is evident; the largest cells contain about 25 tubes while some of the smallest cells include

only three tubes. Note, in particular, that additional detail was added near the bundle periphery (IY=11-13 to more closely model the inner radius tubes (rows ≤ 15). For this same reason, several thin axial layers of cells were included in the U-bend above the top tube support (Figure 7-2, IZ=19 to IZ=25) to more closely model the flow conditions in the area of interest. Note also that a narrow ring of flow cells was specified to represent the bypass flow area in the annulus between the bundle periphery and the wrapper (IY=14).

7.3 ATHOS Results

The results from the ATHOS analysis consist of the thermal-hydraulic flow parameters necessary to describe the 3-D flow field on the secondary side of the steam generator (velocity, density, and void fraction) plus the distributions of the primary fluid and mean tube wall temperatures. The secondary side mixture velocity is composed of three components (V_x , V_y , and V_z) which ATHOS computes on the surfaces of the flow cell. Since the local gap velocity surrounding a tube is required in the vibration analysis, a post-processor is used which: a) interpolates among the velocity components for the cells located nearest to the tube of interest and, b) accounts for the minimum flow area between tubes to calculate the tube-to-tube gap velocity. The post-processor performs the necessary interpolations to determine both in-plane and out-of-plane gap velocities at specific intervals along the length of a tube. It also interpolates on the ATHOS cell-centered density and void fraction to determine the required local parameters along the tube length. The output of the post-processing is a data file which contains these parameter distributions for all the tubes in the generator and which provides a portion of the input data required for tube vibration analyses.

Figure 7-4 shows a vector plot of the flow pattern on the vertical plane of symmetry of the steam generator (the vectors are located at the center of the flow cells shown in Figure 7-2). It is seen that in the U-bend region the mixture turns radially outward, normal to the curvature of the bends toward the region of least flow resistance (i.e., outside the dome formed by the U-bends). Also, because of higher heat flux and void generation, the velocities in the hot leg are higher than in the cold. This difference persists up to the entrance to the U-bend as indicated by the velocity contours shown in Figure 7-5. Here, the axial component of velocity in the hot leg is

about 50% higher than in the cold leg. This figure also indicates the high axial flow component which has just exited the three tubelane flow slots in the top tube support plate. The lateral velocity component, $V_r = \sqrt{V_x^2 + V_y^2}$, in the same horizontal plane (Iz=19) is shown in Figure 7-6. Comparing Figures 7-5 and 7-6, it is seen that at the entrance to the U-bend the vertical velocity component is several times higher than the lateral velocity component in both the hot and cold legs.

Figure 7-7 presents a plot of the void fraction contours on the vertical plane of symmetry of the steam generator. It is evident that the void fraction develops rapidly on the hot leg side of the lower tube bundle. The higher voids in the hot leg continue up into the U-bend where the void fraction varies from about 0.85-0.9 in the hot leg and from 0.65 to 0.85 in the cold leg.

Figures 7-8, 7-9 and 7-10 provide a sample of the individual tube gap velocity and density distributions as computed by the ATHOS post-processor. Results for three Row 10 tubes are plotted. In each figure the gap velocity and density along the length of the tube are plotted from the hot leg tubesheet on the left side of the figure to the cold leg end on the right.

Figure 7-11 presents a plot of the average in-plane gap velocity normal to the tube and density profiles as a function of the column number along Row 10. The average values were taken as the numerical average of the parameter over the entire 180° span of a U-bend at a given column location. The average velocity is seen to be relatively constant with values ranging from 10.5 to 11.2 ft/sec. Small local increases in velocity are present at about tube columns 12, 25, and 38 which correspond to its locations of the tubelane flow slots in the seventh support plate. The average density shows a gradual increase from the bundle interior to the periphery.

7.4 Relative Stability Ratio Over Operating History

One aspect of the evaluation of the Beaver Valley Unit 2 steam generators is to examine the operating history data and use it to determine the susceptibility to fatigue from fluidelastic vibration resulting from the 15 months of operation. This assessment has been completed through the use of a parameter

termed the normalized stability ratio. The normalized stability ratio compares the fluidelastic stability ratio for each period of a plant's operation (fuel cycle) to a reference stability ratio typically based on a recent operating condition. A plot of this ratio against operating time, therefore, provides a relative indication of the effect of past operation on the plant's fluidelastic stability ratio. This normalized time-dependent ratio is subsequently combined with an absolute stability ratio for the reference operating conditions derived from detailed three-dimensional thermal/hydraulic and tube vibration calculations. High values for the net stability ratio, in particular, over a significant period of operation, coupled with other prerequisite conditions (e.g., absence of AVB support and denting at the top tube support plate), could indicate an increased susceptibility to fluidelastic vibration instability and fatigue.

The fluidelastic stability ratio is defined as the ratio of the effective fluid velocity acting on a given tube to the critical velocity at which large amplitude fluidelastic vibration initiates:

$$\text{Fluidelastic Stability Ratio, SR} = \frac{U_{\text{effective}}}{U_{\text{critical at onset of instability}}} \quad [1]$$

In this ratio, the effective velocity depends on the distribution of flow velocity and fluid density, and on the mode shape of vibration. The critical velocity is based on experimental data and has been shown to be dependent upon the tube natural frequency, damping, the geometry of the tube, the tube pattern, and the fluid density, along with the appropriate correlation coefficients.

The detailed calculation of this ratio using velocity and density distributions, etc., requires three-dimensional thermal/hydraulic and tube vibration calculations which are time consuming. Alternately, a simplified, one-dimensional version of this ratio has been used to provide a relative

assessment technique for determining the effect of past operation on the stability ratio. The normalized stability ratio is defined by the following equation:

$$\frac{SR_{cyc\ x}}{SR_{ROP}} = \frac{(\rho V^2)^{1/2}_{cyc\ x}}{(\rho V^2)^{1/2}_{ROP}} * \frac{(m_{ROP})^{1/2}}{(m_{cyc\ x})^{1/2}} * \frac{f_{n\ ROP}}{f_{n\ cyc\ x}} * \frac{(\delta_{ROP})^{1/2}}{(\delta_{cyc\ x})^{1/2}} \quad [2]$$

In this equation "cyc x" refers to each fuel cycle and "ROP" to the recent operating condition. While this simplified approach cannot account for three-dimensional tube bundle effects, it does consider the major operational parameters affecting the stability ratio. Four components make up this ratio: a loading term based on the dynamic pressure (ρV^2), a tube incremental mass(m) term, the natural frequency of the tube (f_n), and a damping ratio (δ) term. It should be noted that the ratio is relative, in that each component is expressed as a ratio of the value for a given fuel cycle or power level to that of the recent operating point.

[

]a,c. The particular damping correlation which is used for all normalized stability ratio calculations is based on a dented condition at the top tube support plate (a clamped condition, as discussed in Section 5.2). The clamped condition is also assumed in calculating the tube natural frequency.

As discussed previously in Section 7.1, the reference three-dimensional stability ratio calculation for the Beaver Valley Unit 2 steam generators was based on a set of full power operating parameters which provided some added margin to the analysis, compared to the available plant data. These same conditions were the basis for the reference components in the 1D normalized stability ratio calculation, labeled "ROP" in equation 2.

Relative stability ratio calculations were completed for this Beaver Valley Unit 2 full power condition and for two lower power levels, 90 and 95% of full power. Since tube vibration and possible fatigue are associated with operation at close to 100% power, only the higher power operating periods are considered important to the evaluation. The high power operating experience for Beaver Valley Unit 2 is summarized in Table 7-2. Note that, since the plant is just completing its first fuel cycle, it has accumulated only a limited period of high power operation. Operation within this first cycle has been grouped within three high power intervals (85-90, 90-95 and 95-100%). Further, it has been conservatively assumed that the total operating time within each of the three power intervals is assigned to the highest power/stability ratio condition in the interval.

The resulting normalized stability ratios for Beaver Valley Unit 2 are shown in Figure 7-12. In this figure, the normalized stability ratio is plotted against cumulative operating time above 85% power. The reference value (=1.00) is for the full power operating condition on which the 3D stability ratios are based. As shown, Beaver Valley Unit 2 has operated only for about 300 days at the reference stability ratio. Operation at the lower power levels has been very limited. The reduced ratios at 90 and 95% power are the combined result of both decreased loading on the tubes and increased damping. Higher damping is a result of lower voids in the U-bend which occurs when the steam pressure rises at reduced power levels. The information shown in Figure 7-12 is utilized in the fatigue evaluation presented in Section 9.0.

References:

- 7-1 L. W. Keeton, A. K. Singhal, et al. "ATHOS3: A computer Program for Thermal-Hydraulic Analysis of Steam Generators", Vol. 1, 2, and 3, EPRI NP-4604-CCM, July 1986.

Table 7-1
Beaver Valley Unit 2 Steam Generator Operating Conditions
Used in the 3D ATHOS Analysis

| | |
|--|--------------------|
| SG Thermal Power (MWT) | 887 |
| Steam Flow Rate (lbm/hr) | 3.87×10^6 |
| Feedwater Inlet Temperature ($^{\circ}$ F) | 437 |
| Steam Pressure (psia) | 811 |
| Water Level (% of span) | 44 |
| Primary Inlet/Outlet Temperatures ($^{\circ}$ F) | 611/542 |
| Circulation Ratio | 4.54 |

Table 7-2
 Beaver Valley Unit 2 Operating History Data
 - Input to Analysis -

| <u>CYCLE</u> | <u>BEG</u> | <u>END</u> | <u>TOTAL</u> <u>DAYS</u> | DISTRIBUTION OF DAYS IN EACH POWER INTERVAL* | | |
|--------------|------------|------------|-----------------------------|---|---------------|---------------|
| | | | | <u>95-100%</u> | <u>90-95%</u> | <u>85-90%</u> |
| 1 | 04-Aug-87 | 11-Oct-88 | 434 | 281 | 5 | 1 |

*Values Input to Analysis

a,b,c

Figure 7-1 Plan View of ATHOS Cylindrical Model for Beaver Valley Unit 2

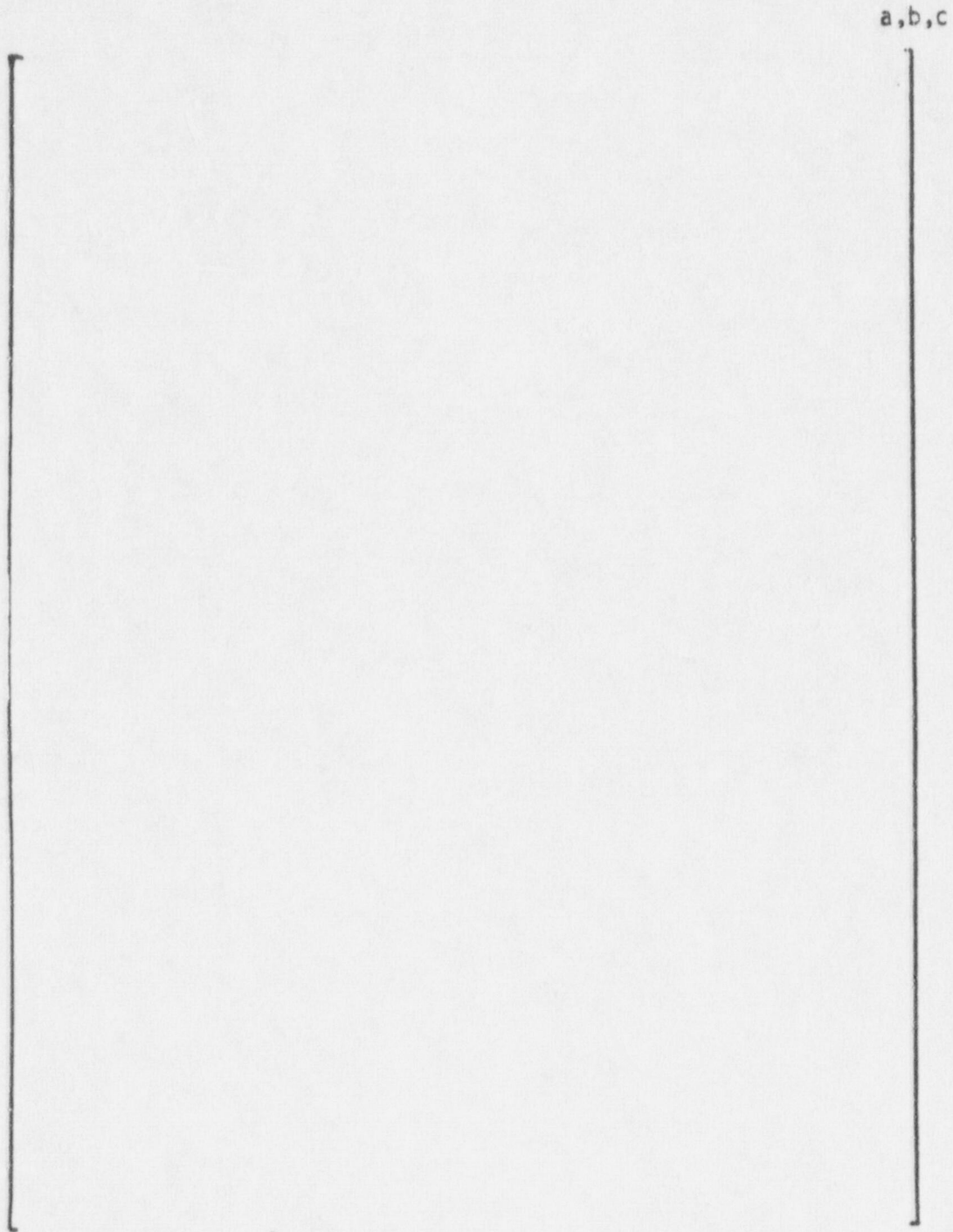


Figure 7-2 Elevation View of ATHDS Cylindrical Model for Beaver Valley Unit 2



Figure 7-3 Plan View of ATHOS Cylindrical Model for Beaver Valley Unit 2
Indicating Tube Layout

a,b,c

Figure 7-4 Flow Pattern on Vertical Plane of Symmetry

a,b,c

Figure 7-5 Vertical Velocity Contours on a Horizontal Plane
at the Entrance to the U-Bend

a,b,c

Figure 7-6 Lateral Flow Pattern on a Horizontal Plane
at the Entrance to the U-Bend

a,b,c

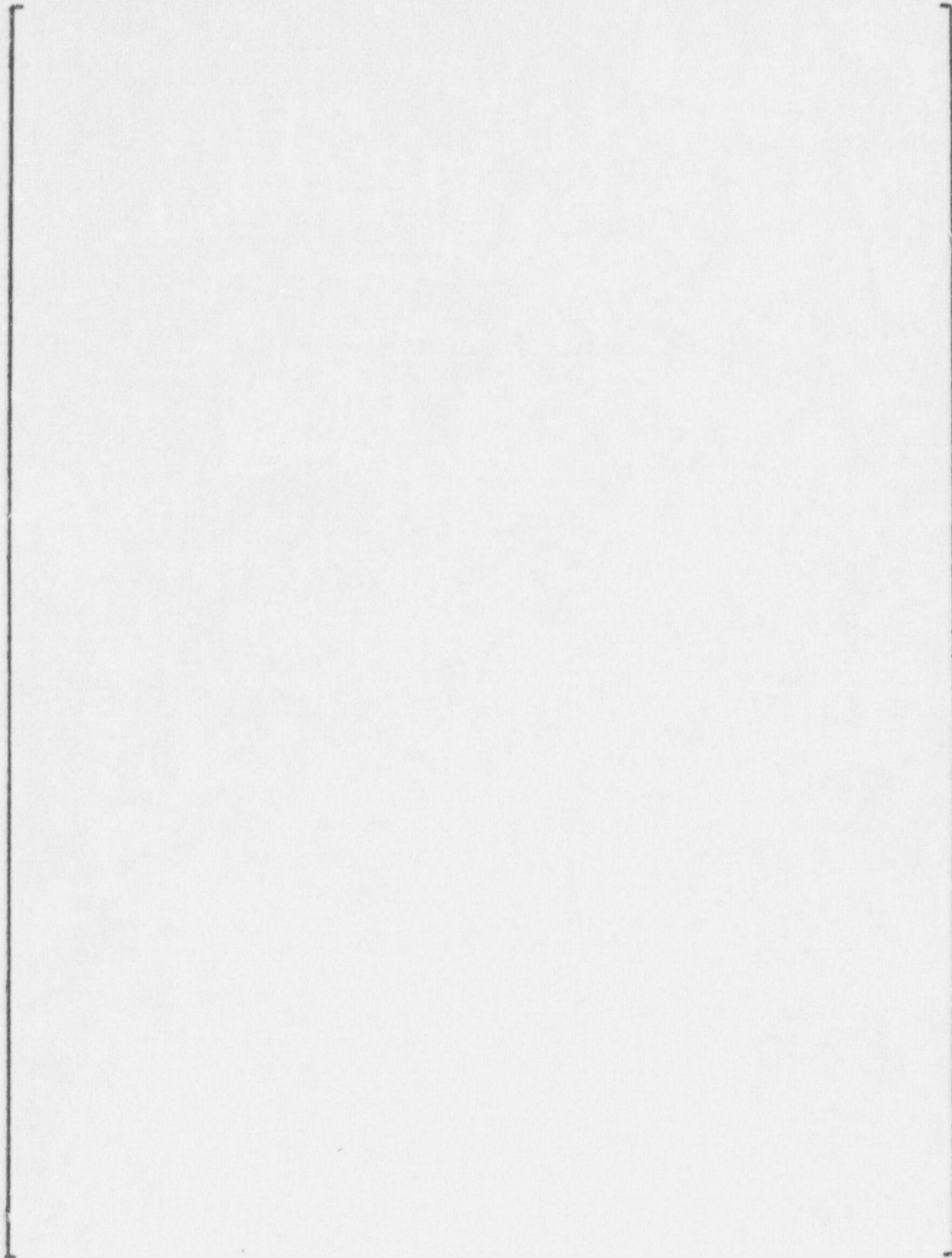


Figure 7-7 Void Fraction Contours on Vertical Plane of Symmetry

a,b,c

Figure 7-8 Tube Gap Velocity and Density Distributions
for Tube Row 10/Column 3

a,b,c

Figure 7-9 Tube Gap Velocity and Density Distributions
for Tube Row 10/Column 20

a,b,c

Figure 7-10 Tube Gap Velocity and Density Distributions
for Tube Row 10/Column 40

a,b,c

Figure 7-11 Average Velocity and Density in the Plane
of the U-Bends Normal to Row 10

a,b,c

Figure 7-12 Beaver Valley Unit 2 Normalized Stability Ratio Based
on High Power (>85%) Operation

8.0 PEAKING FACTOR EVALUATION

This section describes the overall peaking factor evaluation to define the test based peaking factors for use in the tube fatigue evaluation. The evaluation of the eddy current data to define the AVB configuration for North Anna-1 Tube R9C51 is described. This configuration is critical to the tube fatigue assessments as the peaking factors for all other tubes are utilized relative to the R9C51 peaking factor. Uncertainties associated with applying the air model test results to the tube fatigue assessments are also included in this section. Included in the uncertainty evaluation are the following contributions:

- o Extrapolation of air test results to two phase steam-water
- o Cantilever tube simulation of U-bend tubes
- o Test measurements and repeatability
- o AVB insertion depth uncertainty

8.1 North Anna-1 Configuration

8.1.1 Background

The AVB configuration of the ruptured tube in North Anna, R9C51, is the reference case for the tube fatigue evaluations for other plants. In accordance with the NRC Bulletin 88-02, the acceptability of unsupported tubes in steam generators at other plants is based on tube specific analysis relative to the North Anna R9C51 tube, including the relative flow peaking factors. Thus, the support conditions of the R9C51 tube are fundamental to the analyses of other tubes. Because of the importance of the North Anna tube, the support conditions of this tube, which were originally based on "AVB Visible" interpretations of the eddy current test (ECT) data (Figure 8-1), were reevaluated using the projection technique developed since the North Anna event. The projection technique is particularly valuable for establishing AVB positions when deposits on the tubes tend to mask AVB signals such as found for the North Anna 1 tubes. The results of this evaluation are summarized below.

8.1.2 Description of the Method

The basic method utilized was the projection technique in which the AVB position is determined based on measured AVB locations in larger row tubes in the same column. In this study, the projection technique was utilized in the "blind" mode, (AVBs called strictly based on the data) as well as the reverse mode (data examined on the basis of predicted AVB positions). The objective of this application was, with the greatest confidence possible, to establish the positions of the AVBs in an 8 column range around the R9C51 tube in North Anna 1, Steam Generator C.

8.1.3 Data Interpretation

The ECT traces for the U-bends in Rows 8-12 (in one case, 13) were examined for Columns 48-55. The original AVB visible calls are shown in Figure 8-1. The data were examined by an eddy current analyst experienced in reading these traces, and by a design engineer knowledgeable in the geometry of the Model 51 U-bend region.

The intent of this review was to determine if the presence or absence of AVBs as shown in Figure 8-1 could be confirmed using the AVB projection technique. Preliminary projected AVB positions were based on geometric data provided for a few of the tubes near R9C51. The features which were sought were evidence of data "spikes" where AVBs were predicted, offset indications (multiple spikes) where offset AVBs were predicted, single indications where single AVB intersections were predicted, etc. The data evaluation method used was a critical examination of the data, which was biased toward the presence of AVBs unless a confident call of "no AVB" could be made, and then checking the consistency of the data among the tubes in a column and against the theoretical data for the predicted AVB positions. [

] ^{a,c}

[

]a,c.

Figure 8-4 is the "AVB visible" map for columns 48 through 55, based on the critical review of the data. It should be noted that the original data interpretations and the review interpretations are consistent.

8.1.4 Projections

The []a,c ECT traces were utilized for projecting the position of the AVBs according to the standard format of the projection method.

The results of the projections are presented in Figure 8-5, which shows a matrix of projections for tube rows 8 through 13 in columns 48 through 55. For many of the tubes, more than one, and as many as three, projection values

are shown. Multiple projections are expected for a tube if the AVBs on either side of the tube are not at the same elevation, or if the upper and lower AVB support that tube. As many as four different projections are possible if it is assumed that the tube is supported by the upper and lower AVBs, and both upper and lower bars are staggered in elevation as shown in Figure 8-2.

The logic in arranging the projection data is based on the following two rules:

Rule 1. The projections of the same AVB based on different tubes in the same column []^{a,c}.

[

] ^{a,c}.

Rule 2. Two adjacent tubes in the same row []^{a,c}. Consequently, the difference in the [

] ^{a,c}.

The implication of this is that if the position (either left or right) of a projected AVB is assumed for a column, then the projections in the adjacent columns are also [

]a,c.

The arrangement of the AVBs as shown in Figure 8-5 satisfies the rules above and is consistent with the rupture of R9C51. The resulting AVB arrangements, based on the projection matrix of Figure 8-5 is shown in Figure 8-6.

8.1.5 Conclusions

The general AVB arrangement surrounding the ruptured tube in North Anna-1, Steam Generator C, which was the basis for the analysis, is confirmed by a detailed critical review of the ECT data. Differences exist in the AVB pattern between tube columns 48-49, in which the AVBs appear to be less inserted than previously indicated. The pattern of Figure 8-6 is the best fit to the rules which were adopted for determining the position of the AVBs, as well as consistent with explanation of the tube failure.

The basis of the review was a projection technique which utilizes data from tubes one or more rows removed from the actual inserted position of the AVB to determine the position of the AVB. The intent of the review was to establish the positions of the AVBs by confirming or eliminating features of AVB alignments such as side to side offsets, etc. of the AVBs adjacent to the tubes. Overall, the conclusions regarding the positions of the AVBs around R9C51 in North Anna-1, Steam Generator C are based on consistency among all the available data.

8.2 Test Measurement Uncertainties

The descriptions of the peaking factor tests and apparatus were provided in Section 5.4. All practical measures were taken to reduce uncertainties. Nevertheless, some still remain and should be properly accounted for. The important parameter measured during testing that has a significant impact on

peaking factor is the air velocity. The air velocity at test section inlet was measured using a []^{a,c}. Based on considerable experience with the use of such instruments, it is known that the magnitude of uncertainty is very small. A []^{a,c} measurement uncertainty is used in this analysis based on past experience.

8.3 Test Repeatability

During the peaking factor testing of AVB configuration, each test was performed at least two times to confirm repeatability. It has been demonstrated that the tests are quite repeatable with the results often falling within 2 or 3% of one another for the repeat tests. An upper bound value of 5% was used in the current uncertainty analysis.

8.4 Cantilever vs U-Tube

A first order estimate can be made of the validity of modeling a U-bend tube by a cantilever tube in tests to determine the effects of AVB insertion depth on the initiation of fluidelastic vibration. The following assumptions are used:

a,c

a,c

[

For the purposes of this estimate, the geometry of the cantilever measuring tube in the air test model is compared with the geometry of a prototypical Row 10 tube. [

|a,c.

The comparison between a U-bend tube and the model tube involve the consideration of an effective velocity associated with the flow perturbation caused by the AVBs. [

]a,c

[

] ^{a,c}. Using these values, the ratio of the effective velocity for the cantilever measuring tube to that for the U-bend tube is about [] ^{a,c} for the case treated.

A similar evaluation can be made for a Row 10 tube that lies in the projection or shadow of an AVB that is inserted to a depth required to support a Row 9 tube. [

] ^{a,c}.
The net result is that the ratio of the effective velocity for the cantilever tube to that for the U-bend tube is about [] ^{a,c}.

These results indicate that, for the particular assumptions used, the cantilever tube model appears to be a reasonable representation of the U-bend with respect to determining relative peaking factors for different AVB configurations. This evaluation also shows that, on the average, the magnitude of the systematic uncertainty associated with the use of cantilever tube to simulate the U-bend is about [] ^{a,c}.

8.5 Air vs Steam-Water Mixture

The local peaking factors from the air tests can be applied to the steam generator steam/water conditions either as a direct factor on the mixture

velocity and thus a direct factor on a stability ratio, or as a factor on the steam velocity only with associated impacts on density, void fraction and damping. This method leads to a reduction in tube damping which enhances the peaking factor compared to the direct air test value. For estimating an absolute stability ratio, this application of the peaking factor is a best estimate approach. However, for the evaluation of tubes relative to stability ratio criteria, it is more conservative to minimize the peaking factor for the North Anna Unit 1 tube R9C51 through direct application of the air test peaking factor. This conservative approach is therefore used for evaluating tube acceptability.

Under uniform AVB insertion (or aligned AVB insertion), there are no local open channels for flow to escape preferentially. Therefore, air flow is approximately the same as steam/water flow relative to velocity perturbations. Under non-uniform AVB insertion the steam/water flow may differ from air, as the steam and water may separate from each other when an obstruction, such as an AVB, appears downstream. The water would continue along the same channel while steam readily seeks a low resistance passage and thus turns into adjacent open channels. Two phase tests indicate a tendency for steam to preferentially follow the low pressure drop path compared to the water phase.

Based on the above discussion, the F_i are considered to more appropriately apply to the steam phase. Thus, it follows that mixture mass velocity for the tube subject to flow perturbation can be written as follows:

$$\left[\begin{array}{c} \\ \\ \\ \\ \end{array} \right]^{a,c}$$

where D_g is the vapor density, D_f the water density, F_a the velocity peaking factor determined from air tests, j_g^* the nominal superficial vapor velocity, and j_f^* the superficial water velocity. Steam quality can then be determined as follows:

$$\left[\quad \quad \quad \right]^{a,c}$$

The Lellouche-Zolotar correlation (algebraic slip model), as used in the ATHOS code, is applied to determine void fraction. Subsequently, mixture density, velocity and damping coefficients for the tube which is not supported and subject to flow perturbation is evaluated. Therefore, similar to the air velocity peaking factor, local scaling factors of mixture density and velocity and damping coefficient can be readily determined. Finally, a local stability peaking factor for fluidelastic vibration can be calculated as follows:

$$\left[\quad \quad \quad \right]^{a,c}$$

where F_s is the stability peaking factor, F_d the density scaling factor, F_v the velocity scaling factor, and F_{dp} the damping coefficient scaling factor. If we use the air velocity peaking factor without translating to steam/water conditions, then

$$\left[\quad \quad \quad \right]^{a,c}$$

As shown in Table 8-1 stability peaking factors for the steam/water mixture are slightly higher than air velocity peaking factors. The difference between the steam/water and air peaking factors increases as the air peaking factor increases.

For application to tube fatigue evaluations, the ratio of the peaking factor for a specific tube to that for North Anna R9C51 is the quantity of interest. Larger values for this ratio are conservative for the tube fatigue assessment. The North Anna R9C51 peaking factor is one of the highest peaking factors. As discussed in Section 8.7, a peaking factor of nearly $\left[\quad \right]^{a,c}$ is determined for the R9C51 tube. The differences between $\left[\quad \right]^{a,c}$.

$\left[\quad \right]^{a,c}$. Typical values are shown in Table 8-2. These results show

that the direct application of the air test data yields the higher relative peaking factor compared to R9C51. To obtain conservatism in the peaking factor evaluation, [

]a,c.

Comparing the values in the first and last columns of Table 8-1, it may be noted that the stability peaking factor for steam water is []a,c higher than the air velocity peaking factor. On the average, the uncertainty associated with the conservative use of air velocity peaking factor is []a,c.

The conclusion that peaking factor for steam water flow would be higher due to the dependency of damping ratio on void fraction was supported by an alternate study. In this study, a section of steam generator tubes were simulated using the ATHOS code under prototypic flow conditions. The objective of this study was to examine the magnitude of the changes in void fraction and thus stability ratio as a consequence of non-uniform AVB insertion patterns. The current version of ATHOS has modeling limitations that prevent accurate modeling of local geometry effects. In addition, it is believed that an analysis using two-fluid modeling procedure is mandatory to a calculation of the peaking factors for a steam generator to account for the preferential steam flow along the low resistance path. Consequently, the intent of this analysis is only to help bound the uncertainty on void fraction effects from extrapolating the air tests to steam-water.

First the analysis was conducted with uniformly inserted AVBs in the ATHOS model. The ATHOS results were processed by the FLOVIB code to determine stability ratios for the specific tubes of interest. The calculation was repeated using a non-uniform AVB insertion pattern in the model. The results show that the void fraction distribution changes as a result of flow perturbation. Further, the impact on stability ratio resulting from the changes in void fraction profiles was about []a,c. This alternate calculation provides independent corroboration of the prior discussion regarding the stability peaking factors under steam-water conditions vs in air.

8.6 AVB Insertion Depth Uncertainty

The most significant uncertainty for the low peaking configurations is not in the test results, but in the determination of actual AVB insertion patterns adjacent to specific tubes. The methodology used for obtaining the AVB insertion patterns from eddy current data can ascertain the AVB location only to within approximately [

] ^{a,c}. The effect on peaking factor resulting from this uncertainty is addressed using test results of AVB configurations that varied from one another by up to [] ^{a,c}.

Based on maps of AVB insertion depth of various plants, several configurations have been tested for determining fluidelastic instability flow rate by an air cantilever model. Stability peaking factors were then determined from the ratio of critical flow rate for a uniform AVB insertion configuration to a specific configuration. Figure 8-7 summarizes the AVB configurations tested.

Position of AVB insertion depth is determined from Eddy Current Test (ECT) data. Positioning of AVB from ECT data reading is subject to uncertainty; its accuracy is probably about [] ^{a,c}. A change of an AVB insertion depth in a given configuration leads to a different configuration, and thus a different peaking factor. A review of the tested AVB type has been made and results summarized in Table 8-3. As can be seen, a decrease in depth of an appropriate AVB tends to decrease the peaking factor, for instance, a [

] ^{a,c}. Such a trend can be explained; a decrease in a specific AVB depth will open up more channels for incoming fluid to distribute and thus less flow perturbation. However, this applies only to those changes without inducing the reinforcement of flow perturbation from upstream to downstream.

On the average, the uncertainty in peaking factor resulting from small variations in AVB insertion (of the order of 1/2 tube pitch) is found to be [] ^{a,c}.

8.7 Overall Peaking Factor with Uncertainty

As discussed in the previous subsections, there are several aspects to be considered in applying the laboratory test data to steam generator conditions. These considerations were reviewed one at a time in those subsections. This section will integrate the pieces into one set of stability peaking factors.

Looking forward to how these peaking factors are used in the analysis (Section 9), the relative stability ratio calculated for a given tube without the consideration of flow peaking is corrected using the ratio of the peaking factor of the specific tube to that of the North Anna R9C51 tube (Configuration 1a).

It is to be noted that the test results would be applied as ratios of a specific tube peaking factor to the R9C51 peaking factor. This will reduce the influence of some uncertainties since the systematic uncertainties would affect both the numerator and the denominator in the ratio of peaking factors. The major difference will be in those configurations whose peaking factors are significantly lower than that of R9C51. The approach employed here is intended to provide that conservative peaking factors are employed for such apparently low peaking configurations.

The uniform AVB configuration (2a) is selected as a reference configuration, and the peaking factors of all configurations tested are recomputed on the basis of this reference. As discussed below, some of the test uncertainties are applied to the reference case to account for its significantly low peaking relative to the R9C51 configuration.

The uncertainties in the test results and their extrapolation are those due to test measurements, test repeatability, cantilever tubes in the test vs U-tubes in the steam generator, and air tests vs steam-water mixture. These were discussed in more detail in the previous subsections. The magnitude of these uncertainties are listed in Table 8-4.

Of these uncertainties, those due to measurement and repeatability of tests are random errors and can occur in any test. Therefore, these are treated together. The total random uncertainties are calculated by []^{a,c}. The RSS value of these is []^{a,c}. Since these can occur in any test, these are to be applied to all tests. One way of doing this is to apply it to the R9C51 value, that being in the denominator of the final peaking factor ratio. Thus the peaking factor for configuration 1a (R9C51) is reduced by this amount to yield a value of []^{a,c} instead of the []^{a,c} appearing in Table 5-2.

The next three uncertainties in Table 8-4 are systematic uncertainties. It could be argued that these appear in the peaking factors of both the specific tube under consideration and the R9C51 tube and are therefore counter balanced. However, the relative magnitude of these may be different, particularly for configurations with much lower peaking than R9C51. Therefore it was judged that the []^{a,c}.

[]^{a,c}. Similarly, as noted above, the effect on peaking factor due to the uncertainty in the field AVB configuration is also included in this reference case. Thus, []^{a,c}. The peaking factor of the reference configuration 2a (Table 8-5) is raised by this amount to a value of []^{a,c}.

The change in peaking factors of configurations 1a and 2a resulting from the application of uncertainties as described above are shown in Column 3 of Table 8-5. The peaking factors of all configurations are recomputed on the basis of this reference configuration (2a). These values are displayed in Column 4 of Table 8-5.

Some of the uncertainties were applied to the reference configuration (2a) in order to apply them to all low peaking configurations conservatively. Thus, no configuration should have a lower peaking factor than this reference configuration. Therefore, when a peaking factor value less than []^{a,c} is calculated for any configuration, (in Column 3 of Table 8-5), it should be altered to []^{a,c}. Further, for some of the configurations that are conceptually similar, the more limiting (higher) value is used. For example,

a peaking factor of []^{a,c} is used for configurations 5a and 5b based on their similarity to configuration 5c.

The final stability ratio peaking factors calculated on this basis (with configuration 2a as the reference) are shown in Table 8-6.

The overall conclusions from the peaking factor assessment are:

1. As noted in Table 8-4, five elements have been included in the uncertainty evaluation for the peaking factors. The uncertainty estimates were developed from both test and analysis results as described in Sections 8.2 to 8.6. The largest single uncertainty of []^{a,c} is attributable to uncertainties of up to []^{a,c} on determination of AVB insertion depths from field eddy current data. This relatively large uncertainty is applicable only to low peaking conditions where the AVB uncertainties can contribute to small peaking factors. The definition of "no flow peaking" was increased to encompass the small peaking effects from AVB insertion uncertainties. For the AVB patterns leading to significant peaking factors, AVBs were positioned within uncertainties to maximize the peaking factor. For these configurations, variations of AVB insertion within these uncertainties are expected to reduce the peaking factor compared to the final values of Table 8-6 and Figure 8-7.
2. Including uncertainties directed toward conservatively decreasing the peaking factor for the North Anna tube R9C51, the final R9C51 peaking factor is []^{a,c} relative to a no flow peaking condition such as with uniform AVB insertion depths.

8.8 Peaking Factors for Specific Tubes

Peaking factors for Beaver Valley Unit 2 were determined using the methodology described above. Table 8-7 summarizes the results of peaking factors. The AVB positions on each insertion pattern of Figure 8-7 should be carefully noted. Where the AVBs are shown at the top of the test tube, (configurations 4h, 4n for example), the AVBs at least partially block the

flow past the test tube and low flow peaking factors are typically obtained. Where the AVBs are shown at the centerline of the tube row above the test tube, the flow past the test tube is not restricted and significant flow peaking can be obtained.

In applying the methodology to Beaver Valley 2, maps of the AVB insertion depths shown in Figures 6-2 through 6-4 were first reviewed. The second step was to identify those unique and meaningful configurations of AVB insertion depths in locality. In doing so, maximum allowable flow peaking factors were also reviewed column by column for rows 8 through 12. Based on the Beaver Valley 2 tube vibration analysis, flow peaking factors on the order of []^{a,c} for row 8 tubes and []^{a,c} for row 9 tubes would be required for tube fatigue to be a concern.

After conservative estimates of peaking factors were made for specific tubes, those having peaking factors near the maximum allowable value were identified and AVB insertion depth accuracy was reviewed for the tube involved and its neighboring tubes. If needed, stability velocity for the tube with the identified configuration of the AVB insertion depth was determined using the Westinghouse R&D Cantilever, Air Model. Peaking factor was then calculated using the stability velocity.

Determination of peaking factors for identified tubes shown in Table 8-7 are described in detail below. Table 8-7 is broken into small tables for ease in following the description.

8.8.1 Steam Generator A

The following table gives the peaking factors for tubes with unique configurations of AVB insertion depths.

| Steam Generator | Row No | Column No | Type of AVB Insertion Depth | Peaking Factor |
|-----------------|--------|-----------|-----------------------------|--------------------|
| A | 8 | 60 | -4f, <4v | [] ^{a,c} |
| | | 35, 24 | 4a | |
| | 9 | 84, 83 | -7c | |

For R8C60 tube, type 4f may be applicable and type 4v can be used as an upper bound. For R8C35 and R8C24 tubes, type 4a was a conservative choice and a peaking factor of []^{a,c} resulted. Type 7c was a conservative configuration for R9C84 and R9C83 tubes and a peaking factor of []^{a,c} was obtained.

8.8.2 Steam Generator B

Row B tubes with unique AVB configurations are listed below together with their peaking factors.

| Steam Generator | Row No | Column No | Type of AVB Insertion Depth | Peaking Factor |
|-----------------|--------|-----------|-----------------------------|--------------------|
| B | 8 | 61 | -5i | [] ^{a,c} |
| | | 60 | -5g | |
| | | 34 | 4b | |

For R8C61 tube, type 5i was selected to provide a peaking factor of []^{a,c}. Type 5g was chosen for R8C60 tube and a peaking factor of []^{a,c} was obtained. As for R8C34 tube, type 4b was a natural choice and a peaking factor of []^{a,c} was obtained.

For Row 9 tubes, it follows that

| Steam Generator | Row No | Column No | Type of AVB Insertion Depth | Peaking Factor |
|-----------------|--------|-----------|-----------------------------|--------------------|
| B | 9 | 90 | 6b | [] ^{a,c} |
| | | 60 | -1z | |
| | | 53 | 4b | |
| | | 5 | 6b | |

For R9C90 tube, type 6b was a good selection and a peaking factor of []^{a,c} was obtained. For R9C60 tube, type 1z was identified and tested in the Westinghouse R&D Cantilever, Air Model. Type 1z yielded a peaking factor of []^{a,c}. Type 4b was a natural choice and a peaking factor of []^{a,c} was obtained for R9C53 tube. For R9C5 tube, it belongs to type 6's configurations, and a peaking factor of []^{a,c} was obtained.

For Row 10 and 11 tubes, three tubes had unique configurations and are listed below.

| Steam Generator | Row No | Column No | Type of AVB Insertion Depth | Peaking Factor |
|-----------------|--------|-----------|-----------------------------|--------------------|
| B | 10 | 91 | -6c | [] ^{a,c} |
| | | 5 | -6d | |
| | 11 | 5 | -6d | |

All of the three tubes belong to the configurations of type 6's, and they have peaking factor of []^{a,c}

8.8.3 Steam Generator C

The following table presents results of peaking factors determined for Row 8 tubes with unique AVB configurations.

| Steam Generator | Row No | Column No | Type of AVB Insertion Depth | Peaking Factor |
|-----------------|--------|-----------|-----------------------------|--------------------|
| C | 8 | 70 | 5b | [] ^{a,c} |
| | | 69 | 5c | |
| | | 61 | -5i | |
| | | 60 | -5g | |

For R8C70 and R8C69 tubes, type 5b and 5c were used to provide a peaking factor of []^{a,c} for them. Type 5i was selected for R8C61 tube and a peaking factor of []^{a,c} was obtained. As for R8C60 tube, type 5g was used to provide a peaking factor of []^{a,c}.

Peaking factors for Row 9 tubes are given in the following table.

| Steam Generator | Row No | Column No | Type of AVB Insertion Depth | Peaking Factor |
|-----------------|--------|-----------|-----------------------------|--------------------|
| C | 9 | 88 | -6d | [] ^{a,c} |
| | | 84 | 6a | |
| | | 43 | 5b | |
| | | 42 | 5c | |
| | | 35 | -1v, -1c | |
| | | 34 | -7c, -1y | |
| | | 33 | -1r | |

Tube R9C88 and R9C84, belong to the configurations of type 6 and have a peaking factor of []^{a,c}. As for R9C43 and R9C42 tubes, type 5b and type 5c were selected for them, respectively, and they all had a peaking factor of []^{a,c}.

AVB configuration for R9C35 was similar to type 1c or 1v, and a peaking factor of []^{a,c} was given based on type 1v, which yields a higher peaking factor than type 1c. For R9C34 tube, type 7c or 1y was selected, and either one yields a peaking factor of []^{a,c}. For R9C33 tube, type 1r was a very conservative choice and a peaking factor of []^{a,c} resulted.

Row 10 and 11 had three tubes having unique AVB configurations; they are listed below together with their peaking factors.

| Steam Generator | Row No | Column No | Type of AVB Insertion Depth | Peaking Factor |
|-----------------|--------|-----------|-----------------------------|--------------------|
| C | 10 | 5 | -5i | [] ^{a,c} |
| | | 4 | -5f | |
| | 11 | 4 | -1r | |

For R10C5 tube, type 5i was selected and a peaking factor of []^{a,c} was obtained while, for R10C4 tube, type 5f was considered and a peaking factor of []^{a,c} was thus given.

For R11C4 tube, type 1r was identified and tested in the Westinghouse R&D Cantilever, Air Model. A peaking factor of []^{a,c} was obtained.

Table 8-2

Comparison of Air and Steam-water Peaking Factor Ratios

| Air Peaking Factor | Air Peaking Ratio | Steam Peaking Factor | Steam Peaking Ratio |
|--------------------------|-------------------------|----------------------------|---------------------------|
|--------------------------|-------------------------|----------------------------|---------------------------|

[

]

a,c

Table 8-3

Effect of Local Variation of AVB Insertion

| Type A | Type B | A to B AVB Variation | Peaking Factor A | Peaking Factor B | Ratio (B/A) | |
|--------|--------|-------------------------|---------------------|---------------------|----------------|------|
| | | | | | | a, c |
| | | | | | | a, c |

Table 8-4

Uncertainties in Test Data and Extrapolation

| | <u>Source of Uncertainty</u> | <u>Type</u> | <u>Magnitude, %</u> |
|----|------------------------------|-------------|---------------------|
| 1. | Velocity measurement | Random | [] ^{a, c} |
| 2. | Test repeatability | Random | |
| 3. | Cantilever vs U-tube | Systematic | |
| 4. | Air vs steam-water mixture | Systematic | |
| 5. | Field AVB configuration | * | |

* This is not an uncertainty associated with the test data. It results from the inaccuracy in determining the true AVB position in the field using eddy current data.

Table 8-5
Extrapolation of Test Results to Steam Generator Conditions

| Configuration | Test Data | Data with Uncertainties | Peaking Factor Referenced to Configuration 2a |
|---------------|-----------|-------------------------|---|
|---------------|-----------|-------------------------|---|

| Configuration | Test Data | Data with Uncertainties | Peaking Factor Referenced to Configuration 2a |
|---------------|-----------|-------------------------|---|
| | | | a, c |

Table 8-6
Final Peaking Factors

| Configuration | Peaking Factor |
|---------------|---|
| 1a | <div style="display: flex; align-items: center; justify-content: center;"> <div style="font-size: 4em; margin-right: 10px;">[</div> <div style="text-align: center;"> <p data-bbox="1123 445 1171 474">a, c</p> </div> <div style="font-size: 4em; margin-left: 10px;">]</div> </div> |
| 1b | |
| 1r | |
| 1v | |
| 1y | |
| 1z | |
| 2a | |
| 4a | |
| 4b | |
| 4f | |
| 4v | |
| 5a | |
| 5b | |
| 5c | |
| 5f | |
| 5g | |
| 5i | |
| 6a | |
| 6b | |
| 6c | |
| 6d | |
| 7b | |
| 7c | |

Table 8-7
Stability Velocity Peaking Factors for Specific Tubes
Beaver Valley 2

| Steam Generator | Row No | Column No | Type of AVB Insertion | Peaking Factor |
|----------------------|----------------------|-----------|-----------------------|----------------|
| A | 8 | 60 | -4f, <4v | [] a, c |
| | | 35, 24 | 4a | |
| | 9 | 84, 83 | -7c | |
| | All of the Remaining | | | |
| B | 8 | 61 | -5i | |
| | | 60 | -5g | |
| | | 34 | 4b | |
| | 9 | 90 | 6b | |
| | | 60 | -1z | |
| | | 53 | 4b | |
| | | 5 | 6b | |
| | 10 | 91 | -6c | |
| | | 5 | -6d | |
| | 11 | 5 | -6d | |
| | All of the Remaining | | | |
| C | 8 | 70 | 5b | |
| | | 69 | 5c | |
| | | 61 | -5i | |
| | | 60 | -5g | |
| | 9 | 88 | -6d, -7b | |
| | | 84 | 6a | |
| | | 43 | 5b | |
| | | 42 | 5c | |
| | | 35 | -1v, -1c | |
| | | 34 | -7c, -1y | |
| | | 33 | -1r | |
| | 10 | 5 | -5i | |
| | | 4 | -5f | |
| 11 | 4 | -1r | | |
| All of the Remaining | | | | |

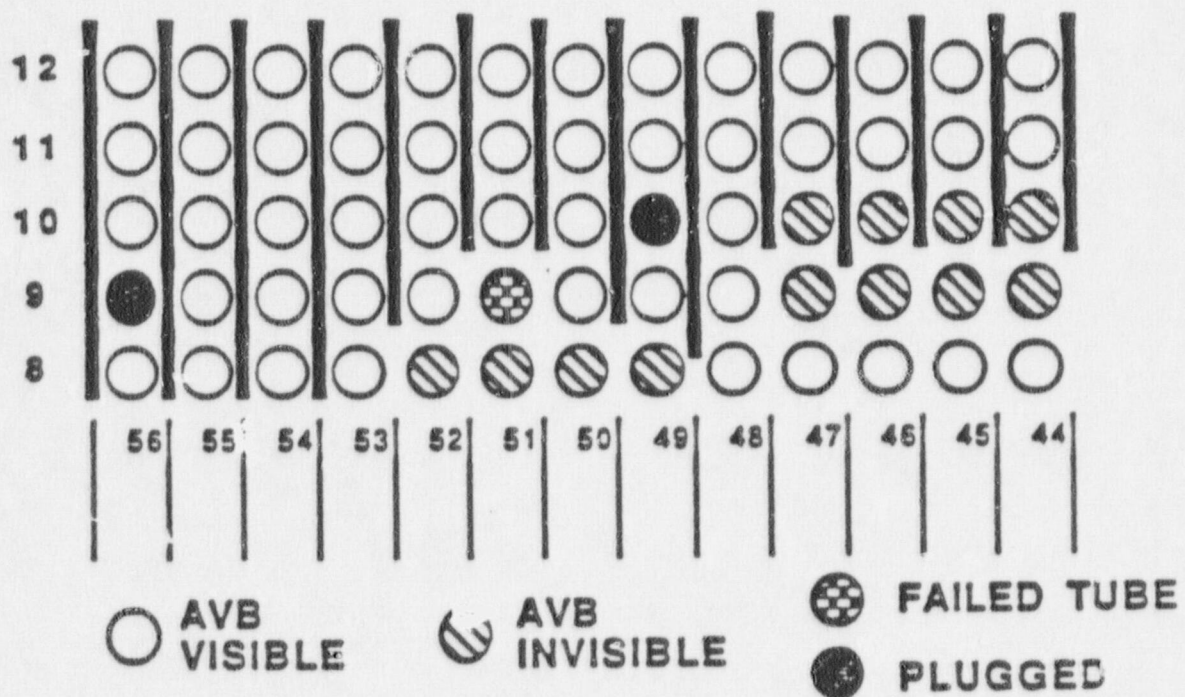


Figure 8-1 Original North Anna AVB Configuration

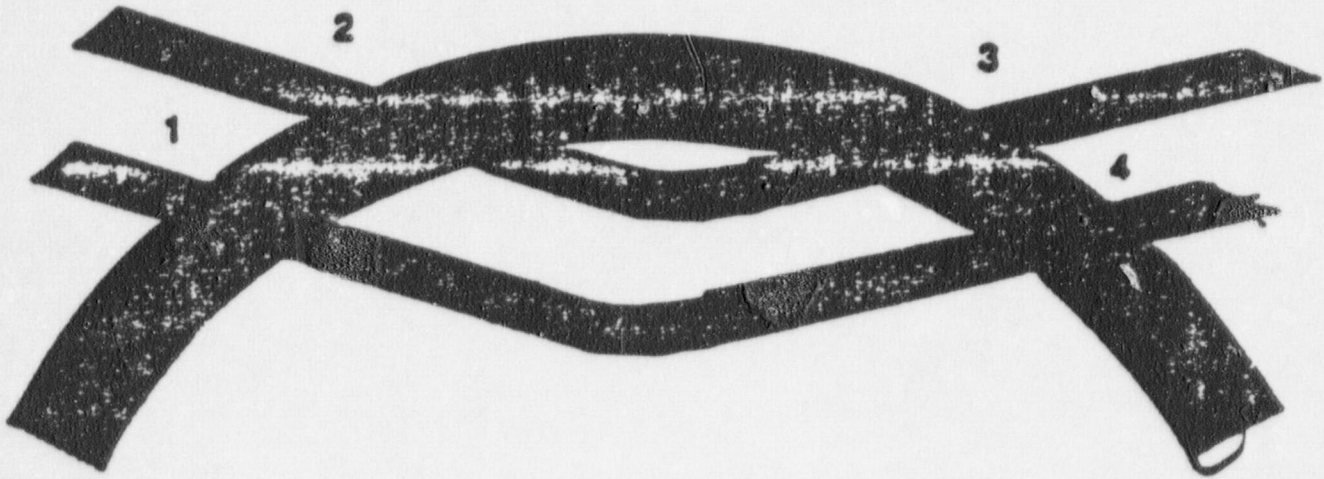


Figure 8-2 Schematic of Staggered AVBs

a, c

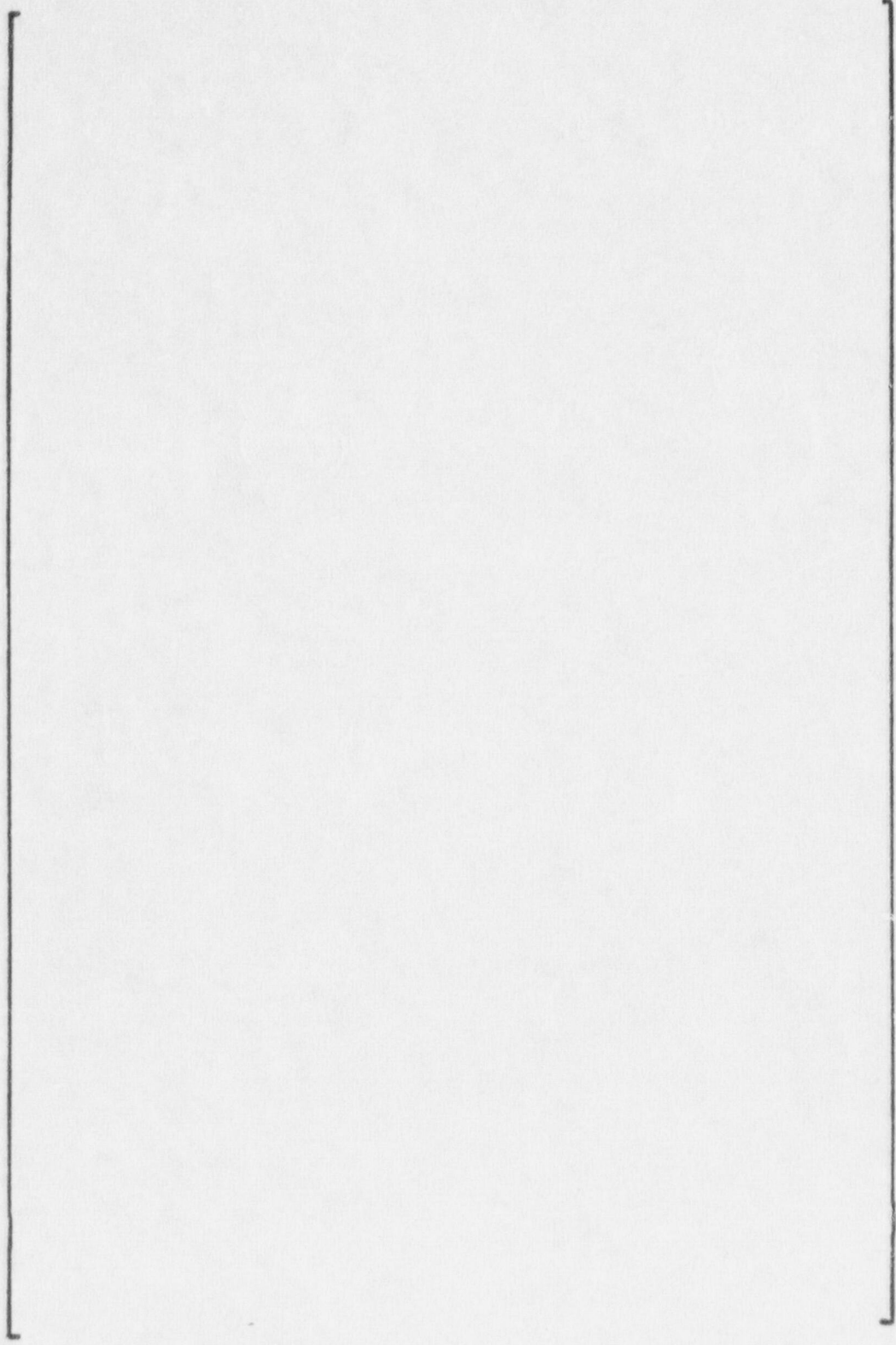
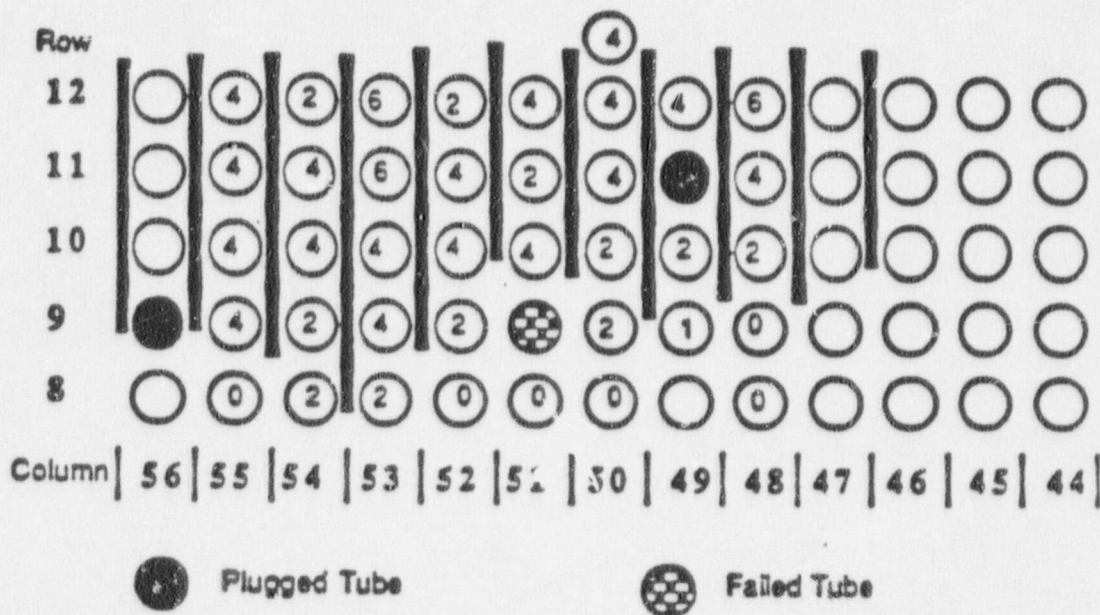


Figure 8-3 AVB "Pair" in ECT Trace



Numbers in circles in column range 48-55 represent readable AVB intersection signals, based on critical review of the ECT traces.. Open circle in this range means no data is available.

Figure B-4 North Anna 1, Steam Generator C, AVB Positions
Critical Review "AVB Visible" Calls

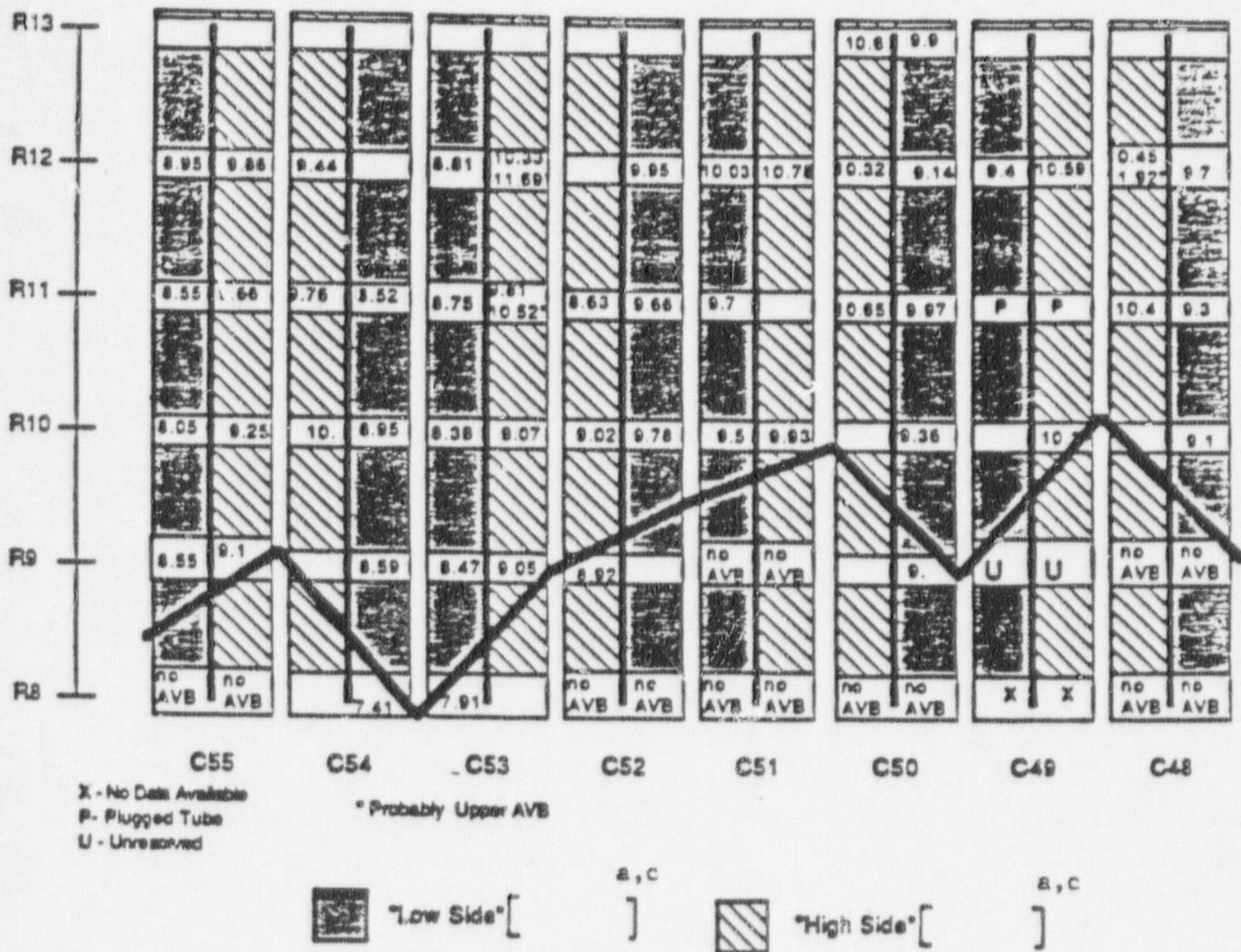


Figure 8-5 North Anna 1, Steam Generator C,
R9C51 AVB []^{a,c} Matrix

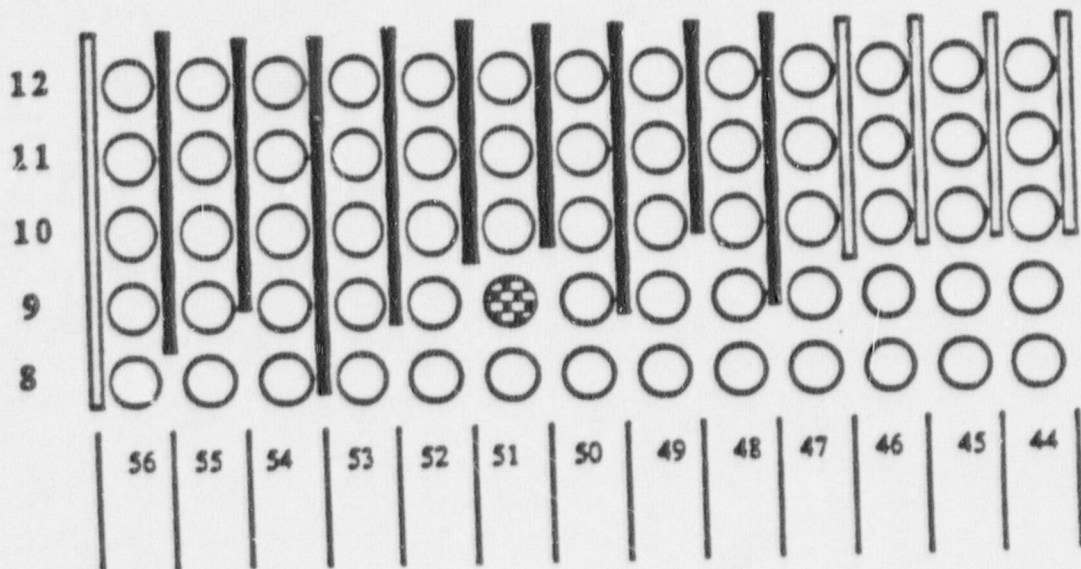


Figure 8-6 North Anna R9C51 AVB Final [^{a,c}] Positions

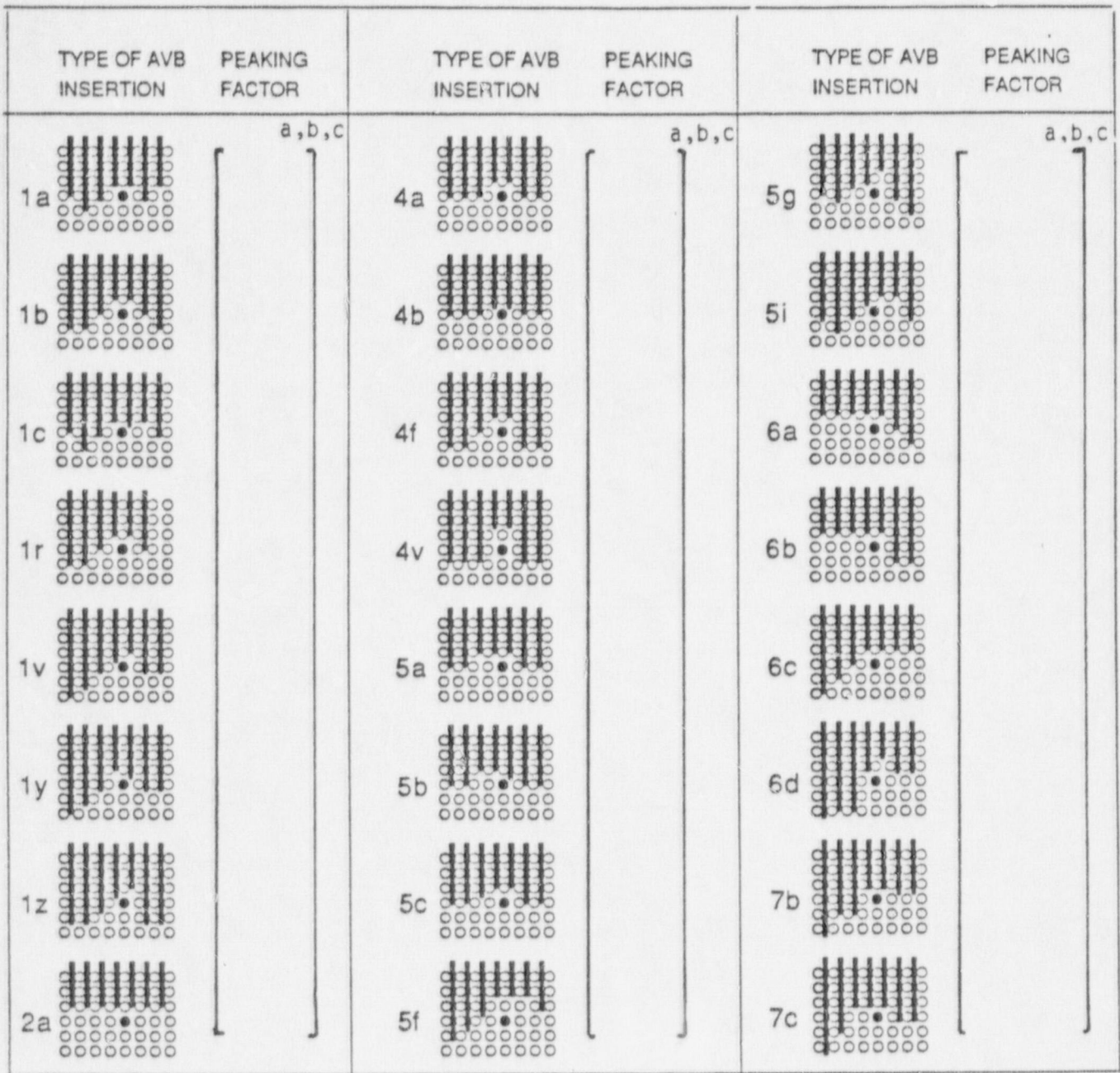


Figure 8-7 Final Peaking Factor for Beaver Valley 2

9.0 STRUCTURAL AND TUBE VIBRATION ASSESSMENTS

9.1 Tube Mean Stress

This section summarizes the analysis to determine stresses in a dented but undeformed tube at 100% power. Loads imposed on the tube correspond to steady-state pressure, differential thermal expansion between the tube and the support plate, and a thru-wall thermal gradient. The analysis assumes the tube to be []^{a,c} at cold shutdown.

A summary of the temperature and pressure parameters at 100% power in the vicinity of the top support plate are provided in Table 9-1. The tube temperature corresponds to the average of the primary-side water temperature and the plate temperature. The resulting tube/plate radial interference is []^{a,c}.

Stresses due to differential pressure and interference loads are calculated using finite element analysis with the model shown in Figure 9-1. The model prescribes [

] ^{a,c}

Two reference cases were run using the finite element model, the first for a primary-to-secondary side pressure gradient of 1000 psi, and the second for a []^{a,c} inch radial interference between the tube and plate. The pressure case incorporates the axial load on the tube by applying a pressure loading along the top face of the model. Plots showing the distribution of stress for the tube outer surface for the two reference cases are provided in Figures 9-2 and 9-3. Thermal bending stresses due to the thru-wall thermal gradient are calculated to be 9.1 ksi using conventional analysis techniques. The combined stress distribution along the tube length, in Figure 9-4, was obtained by combining the thermal bending stresses and the reference solutions with appropriate multipliers based on 100% power operating parameters.

The maximum axial tensile stress is 22.5 ksi and occurs approximately 0.134 inch above the top surface of the support plate. Adding, for conservatism, the surface stress due to pressure, 0.8 ksi, gives an applied mean stress of 23.3 ksi. In addition to the applied stress, residual stresses exist in the tube as a result of the manufacturing process. For mill annealed tubes with subsequent straightening and polishing, residual stresses are compressive at the tube surface, but 5-10 mils below the surface, the stress levels change to 10-15 ksi tensile. Combining the applied and residual stresses results in a cumulative mean stress of approximately 38 ksi, assuming tube denting without deformation.

If a tube is dented with deformation, the mean stress is limited by tube yielding. For the case of dented tubes with deformation, the maximum effect of mean stress was incorporated by using $\sigma_{\max} = \sigma_y$ in determining stability ratios and fatigue usage.

9.2 Stability Ratio Distribution Based Upon ATHOS

An assessment of the potential for tubes to experience fluid elastic instability in the U-bend region has been performed for each of the tubes in rows eight through twelve. This analysis utilizes FASTVIB, a Westinghouse proprietary finite element based computer code, and PLOTVIB, a post processor to FASTVIB. These codes predict the individual responses of an entire row of steam generator tubing exposed to a location dependent fluid velocity and density profile. The program calculates tube natural frequencies and mode shapes using a linear finite element model of the tube. The fluid elastic stability ratio U_e/U_c (the ratio of the effective velocity to the critical velocity) and the vibration amplitudes caused by turbulence are calculated for a given velocity/density/void fraction profile and tube support condition. The velocity, density and void fraction distributions are determined using the ATHOS computer code as described in Section 7.3. The WECAN generated mass and stiffness matrices used to represent the tube are also input to the code. (WECAN is also a Westinghouse proprietary computer code.) Additional input to FASTVIB/PLOTVIB consists of tube support conditions, fluid elastic stability constant, turbulence constants, and location dependent flow peaking factors.

This process was performed for the Beaver Valley Unit 2 steam generator tubes and also for the North Anna Row 9 Column 51 tube (R9C51) using similarly appropriate ATHOS models. Ratios of the Beaver Valley Unit 2 results to those for North Anna Unit 1 R9C51 were generated to produce a quantity that could be used to provide an initial assessment of the Beaver Valley Unit 2 tubes relative to the ruptured tube at North Anna Unit 1.

Figure 9-5 contains the results of this process for each of the rows under investigation. The relative ratios are obtained using the following conditions for Beaver Valley Unit 2 and North Anna Unit 1:

- 1) Tube is fixed at the top tube support plate,
- 2) Void fraction dependent damping,
- 3) No AVB supports are active,
- 4) Location dependent flow peaking factors.

It is to be noted that the stability ratios plotted are composites of all steam generators. That is, any peaking effect for a given tube location on the plot represents the maximum value of the peaking factors in all steam generators at that location.

A horizontal line is drawn at the relative stability ratio value of 0.90. This identifies the point where a ten percent reduction in stability ratio exists relative to North Anna R9C51. (See Section 4.1 for a discussion of the stability ratio reduction criteria.) All the tubes with ratios above this line would be considered to have stability ratios larger than ninety percent of North Anna R9C51.

This figure indicates that most tubes in Rows 8 thru 11 of the Beaver Valley Unit 2 steam generators lie below the 90% line. Note that all of Row 12 is supported and therefore the relative stability ratios presented in this figure for this row can be disregarded.

All unsupported tubes, with the exception of R9C33 SG C and R11C14 SG C, have RSR values (including flow peaking) less than 0.90.

9.3 Stress Ratio Distribution with Peaking Factor

An evaluation was performed to determine the ratio of the Beaver Valley Unit 2 tube stress over the North Anna R9C51 tube stress. This ratio is determined using relative stability ratios discussed in the previous section, relative flow peaking factors (Table 8-7 factors divided by $[\quad]^{a,c}$) and bending moment factors. Sections 4.2 and 4.3 contain additional information and describe the calculational procedure used to obtain the results presented in this section. The results presented below are based upon the following conditions:

- 1) Tube is fixed at the top tube support plate,
- 2) Damping is void fraction dependent,
- 3) Tubes have no AVB support,
- 4) 10% criteria with frequency effects,
- 5) Tubes are assumed to be dented or undented (both situations were considered, but the evaluation is based on the more limiting, dented case).

A tube can be considered acceptable if the stress ratio is less than 1.0 when calculated using the procedure described in Sections 4.2 and 4.3 and including the conditions listed above and subject to confirmation of fatigue usage acceptability. Conformance to these requirements implies that the stress acting on a given tube is expected to be insufficient to produce a fatigue event in a manner similar to the rupture that occurred in the R9C51 tube at North Anna Unit 1.

Figure 9-6 shows the results of the stress ratio calculations for the Beaver Valley Unit 2 tubes in Rows 8 through 12. (Row 12 is included for completeness of evaluation even though all Row 12 tubes were found to be supported). As in

the case of relative stability ratio plots, the plotted stress ratios represent the composite set for all steam generators. These ratios are applicable for tubes that are dented (tube deformation) at the top tube support plate. This case bounds the clamped tube condition with no tube deformation, i.e., the case corresponding to the NRC definition of denting with top tube support plate corrosion plus magnetite in the crevice without tube deformation. With the exception of a very small number of tubes, the current tube conditions at Beaver Valley Unit 2 correspond to this latter definition of denting.

Figure 9-7 contains the results for the case where tube deformation is not present. These two pairs of figures demonstrate the effects of varying the applied mean stress on the tube. Using the reduced mean stress, present in the undented results, produces stress ratio values that are lower than stress ratios calculated for tubes in the dented condition.

As can be observed in Figures 9-6 and 9-7 and Table 9-2, two tubes (R9C33 and R11C4; located in SG C) lay above the 1.00 stress ratio line for both the dented and undented condition at Beaver Valley Unit 2. Final eddy current evaluations have indicated that magnetite was not present at the top TSP during the latest inspection period. Note that all of Row 12 is supported, therefore, the stress ratio presented in the figure, for Row 12 can be disregarded.

As noted in Section 9.5, it is conservatively recommended that all tubes with stress ratios exceeding acceptance criteria of 1.0 be removed from service.

An evaluation has also been performed to determine the required relative flow peaking that will produce a stress ratio not greater than 1.0. Figure 9-8 contains the results of this process for all the tubes in Rows 8 through 12. The figure was generated using the conditions outlined previously with the additional constraint that the tubes are dented. Note that this figure reads opposite of the previous figures, i.e., the top curve in the figure corresponds to Row 8 and the bottom curve corresponds to Row 12. Maximum Allowable Relative Flow Peaking is the required relative flow peaking (0.68 corresponds to no flow peaking) that, if used on the given tube, will produce a stress ratio (with denting) not to exceed 1.0.

This curve can be used to identify the relative flow peaking required before preventive action would be recommended and, when used in conjunction with the actual flow peaking associated with each tube, to determine the margin present. This has also been performed in Table 9-2. The column with heading "Max Allow Flow Peak" identifies the relative flow peaking factor that would be permitted, on a tube by tube basis, before the stress ratio criteria would be exceeded. As can be observed in the table and figure, the inner row tubes have larger values of allowable relative flow peaking when compared to the outer rows.

9.4 Cumulative Fatigue Usage

All tubes that are unsupported and have a stress ratio ≤ 1.0 have a maximum stress amplitude that is < 4.0 ksi (from 9.5 ksi) since a 10% reduction in the stability ratio for the North Anna Row 9 Column 51 tube was the criteria basis. The stability ratios for the Beaver Valley Unit 2 tubing are based on the current operating parameters and with future operation on the same basis, the tubes are not expected to rupture as a result of fatigue if 1) they meet the stress ratio criteria of ≤ 1.0 and 2) their current and future fatigue usage will total less than 1.0.

All tubes in the evaluation have conservatively been considered to be dented with deformation. Based on the above analyses, all Beaver Valley Unit 2 tubes with the exception of R9C33 and R11C04 (both in SG-C) meet the relative stress ratio criteria under the current AVB conditions. Table 9-2 provides a summary of the combined relative stability ratios and the stress ratios for the more salient unsupported tubes in Rows 8 through 12. This table is prepared using the stress and stability ratios in conjunction with individual tube flow peaking ratios and AVB support conditions.

Acceptability of the Beaver Valley Unit 2 tubing for fatigue is accomplished by demonstrating the acceptability of the remaining tube with the highest stress ratio. R9C60 in SG-A. This tube has a stress ratio (if dented) of 0.78. Assuming the tube had been dented since the first cycle and continue to operate under current conditions, the total usage including the remaining term of the operating license would be 0.40. In the event of a future uprating of the plant, the potential for tube fatigue must be re-evaluated.

Table 9-1

100% Power Operating Parameters - Beaver Valley Unit 2
Bounding Values for Mean Stress Calculation

Primary Pressure = 2250 psia
Secondary Pressure = 811 psia
Pressure Gradient = 1439 psi

Primary Side Temperature * = 577°F
Secondary Side Temperature = 520°F
Tube Temperature = 548°F

* Average of $T_{hot} = 611^{\circ}\text{F}$ and $T_{cold} = 542^{\circ}\text{F}$.

Table 9-2

BEAVER VALLEY UNIT 2 - TUBES WITH SIGNIFICANT RSR OR STRESS RATIOS

| S/G ROW | COLUMN | FLOW PEAK | MAX. ALLOW FLOW PEAK | RSR*FP | STRESS RATIO | |
|----------|-------------|-----------|----------------------|--------|--------------|----------|
| | | | | | W DENT | W/O DENT |
| A 8 | 2-18 | 0.68 | A,C | 0.580 | 0.11 | 0.10 |
| | 24,35 | 0.79 | | 0.670 | 0.24 | 0.21 |
| | 39-56 | 0.68 | | 0.570 | 0.10 | 0.09 |
| | 60 | 1.05 | | 0.829 | 0.78* | 0.70* |
| | 79-84,87-90 | 0.68 | | 0.580 | 0.11 | 0.10 |
| B 8 | 2-6 | 0.68 | 0.521 | 0.06 | 0.05 | |
| | 9-15 | 0.68 | 0.580 | 0.11 | 0.10 | |
| | 34,38-57 | 0.68 | 0.570 | 0.10 | 0.09 | |
| | 90-93 | 0.68 | 0.515 | 0.06 | 0.05 | |
| | 60 | 0.76 | 0.537 | 0.13 | 0.12 | |
| | 61 | 0.80 | 0.608 | 0.14 | 0.13 | |
| C 8 | 2-18,25-27 | 0.68 | 0.580 | 0.11 | 0.10 | |
| | 33-35 | 0.68 | 0.537 | 0.07 | 0.06 | |
| | 38-56 | 0.68 | 0.569 | 0.10 | 0.09 | |
| | 60,69,70 | 0.76 | 0.647 | 0.20 | 0.18 | |
| | 61 | 0.80 | 0.608 | 0.14 | 0.13 | |
| | 71,72,77-85 | 0.68 | 0.577 | 0.11 | 0.09 | |
| | 88-93 | 0.68 | 0.535 | 0.07 | 0.06 | |
| A 9 | 2-14 | 0.68 | 0.678 | 0.21 | 0.19 | |
| | 83,84 | 0.68 | 0.677 | 0.21 | 0.19 | |
| B 9 | 2-5 | 0.68 | 0.611 | 0.12 | 0.11 | |
| | 41-50 | 0.68 | 0.667 | 0.19 | 0.17 | |
| | 53,60 | 0.68 | 0.660 | 0.18 | 0.16 | |
| | 90-93 | 0.68 | 0.611 | 0.12 | 0.11 | |
| C 9 | 2-12 | 0.68 | 0.677 | 0.21 | 0.19 | |
| | 33 | 1.08 | 0.944 | 1.35** | 1.20** | |
| | 34 | 0.68 | 0.616 | 0.12 | 0.11 | |
| | 35 | 0.82 | 0.767 | 0.41 | 0.37 | |
| | 42,43 | 0.76 | 0.737 | 0.33 | 0.30 | |
| | 46-55,79-84 | 0.68 | 0.677 | 0.21 | 0.19 | |
| | 88-93 | 0.68 | 0.627 | 0.14 | 0.12 | |
| A 10 | 2,3 | 0.68 | 0.723 | 0.25 | 0.22 | |
| B 10 | 2-5,91-93 | 0.68 | 0.723 | 0.25 | 0.22 | |
| C 10 | 2-3 | 0.68 | 0.723 | 0.25 | 0.22 | |
| | 4 | 0.79 | 0.831 | 0.54 | 0.48 | |
| | 5 | 0.80 | 0.839 | 0.57* | 0.51* | |
| A 11 | None | | | | | |
| B 11 | 2-5 | 0.68 | 0.856 | 0.55 | 0.49 | |
| C 11 | 4 | 1.08 | 1.318 | 434.** | 388.** | |
| A,B,C 12 | None | | | | | |

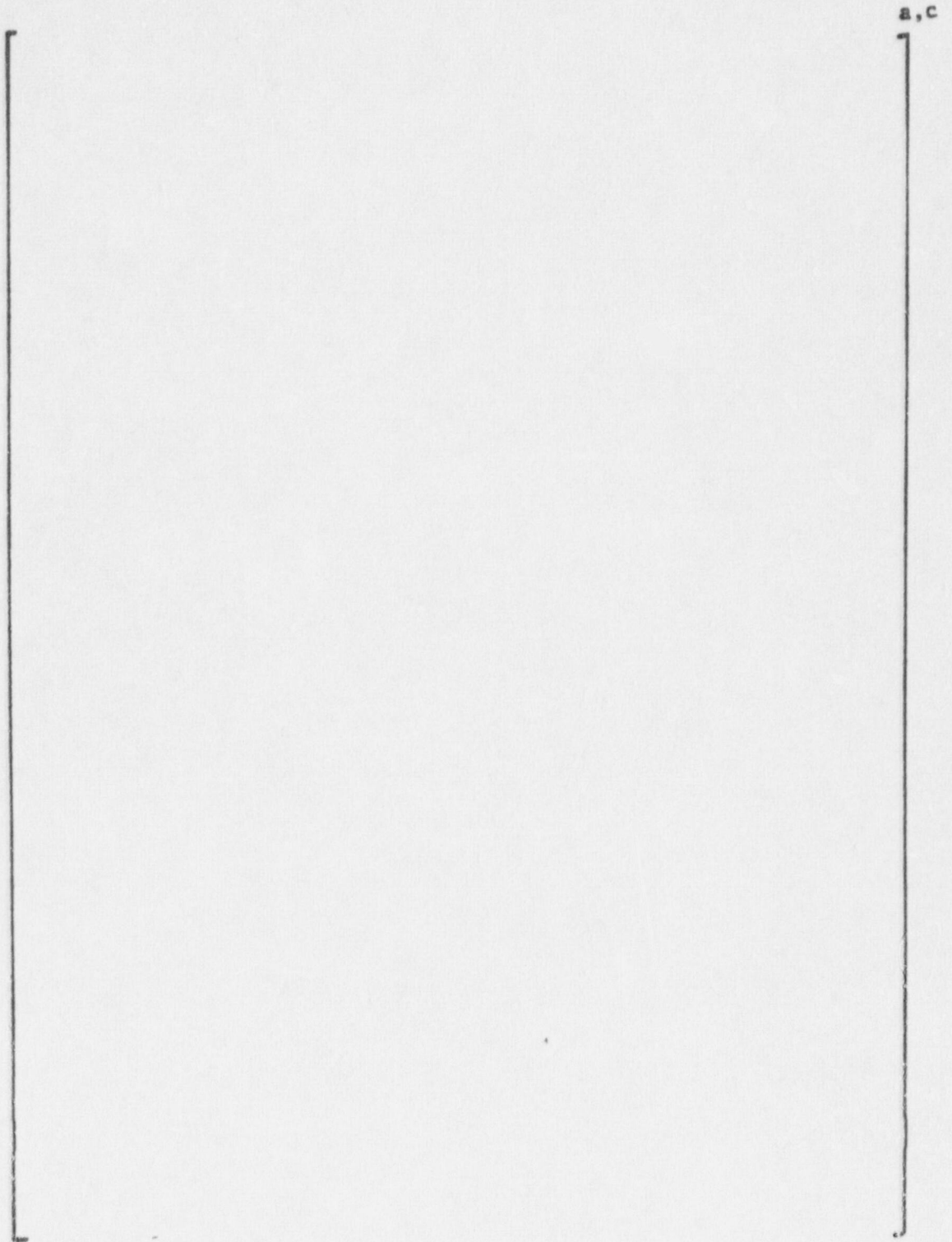


Figure 9-1 Axisymmetric Tube Finite Element Model

B,C

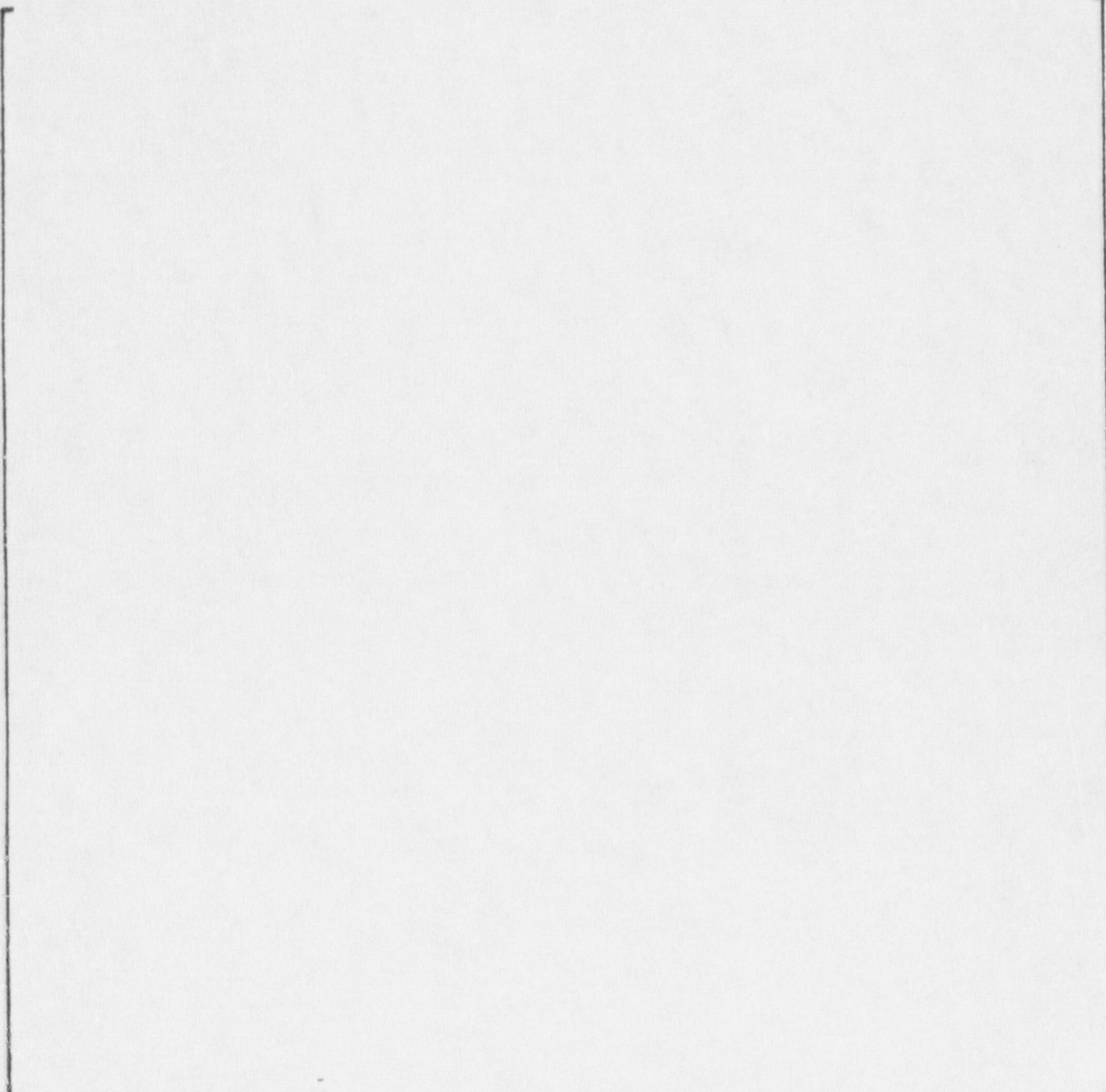


Figure 9-2 Dented Tube Stress Distributions
Pressure Load on Tube

a, c

Figure 9-3 Dented Tube Stress Distributions
Interference Load on Tube

a, c

Figure 9-4 Dented Tube Stress Distributions
Combined Stress Results

a, c



Figure 9-5 Relative Stability Ratios Using MEVF Dependent Damping - Beaver Valley Unit 2 Plant
(Composite of all Steam Generators with Umbrella Flow Peaking)

a, c



Figure 9-6 Stress Ratio vs. Column Number - Dented Condition - Beaver Valley Unit 2 Plant
(Composite of all SGs with Umbrella Flow Peaking)

a, c

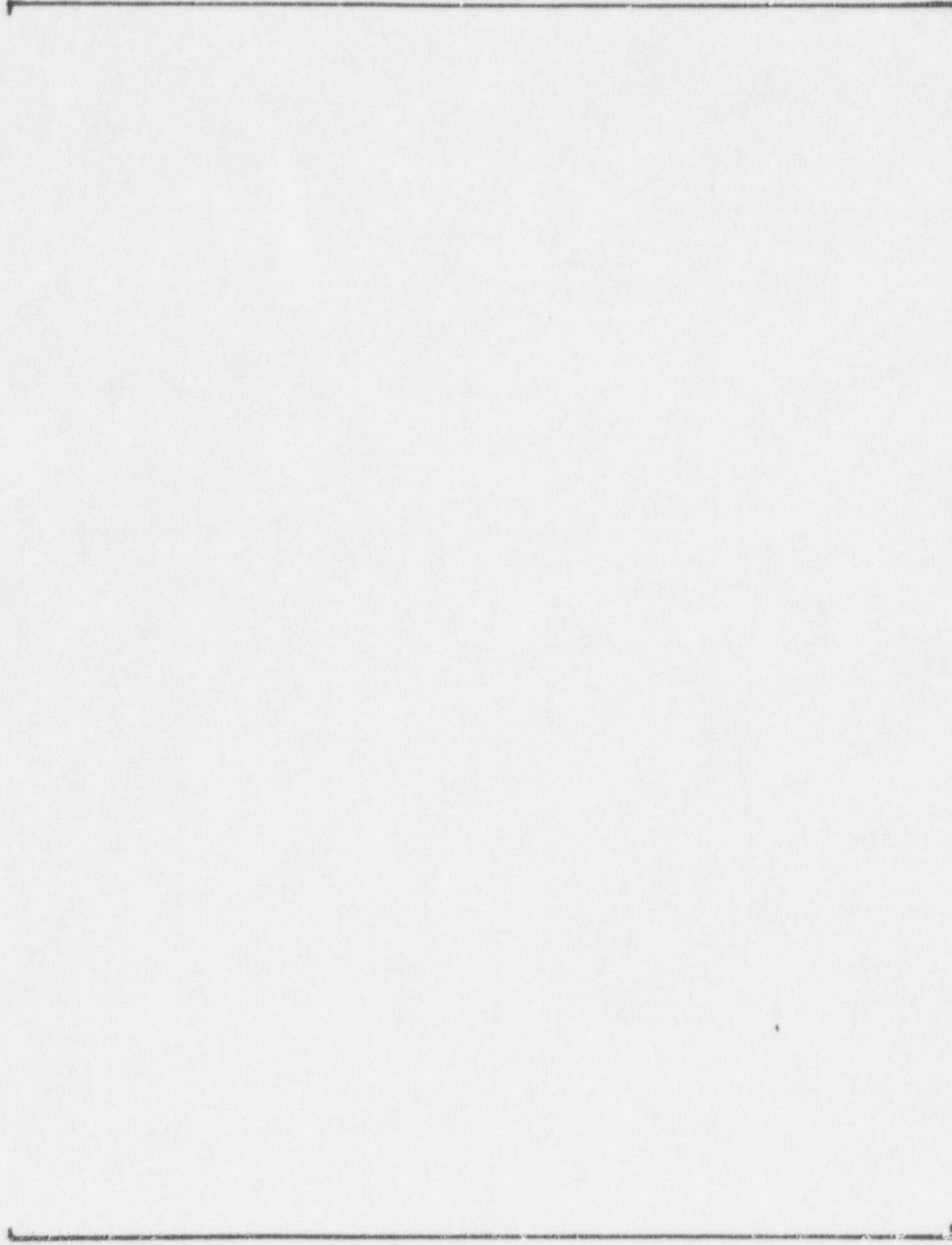


Figure 9-7 Stress Ratio vs. Column Number - Undented Condition - Beaver Valley Unit 2
(Composite of All SGs with Umbrella Flow Peaking)

a,c



Figure 9-8 Beaver Valley Unit 2 - Maximum Allowable Relative Flow Peaking